Vol. 53: 67–87, 2024
https://doi.org/10.3354/esr01286

ENDANGERED SPECIES RESEARCH
Endang Species Res

Published February 1

Contribution to the Special 'Global status of wedgefish and guitarfish'

Review of three southwestern Indian Ocean species of *Rhinobatos* (Rhinopristiformes: Rhinobatidae)

Rachel M. Aitchison[1,*], David A. Ebert[1,2,3], Bernard Séret[4], Simon Weigmann[5,6]

[1]Pacific Shark Research Center, Moss Landing Marine Laboratories, San Jose State University, Moss Landing, CA 95039, USA
[2]Research Associate, Department of Ichthyology, California Academy of Sciences, San Francisco, CA 94118, USA
[3]Research Associate, South African Institute for Aquatic Biodiversity, Grahamstown 6140, South Africa
[4]IchtyoConsult, 6 bis rue du Centre, 91430 Igny, France
[5]Elasmo-Lab, Elasmobranch Research Laboratory, Sophie-Rahel-Jansen-Str. 83, 22609 Hamburg, Germany
[6]Leibniz Institute for the Analysis of Biodiversity Change (LIB), Centre for Taxonomy and Morphology, Zoological Museum, Martin-Luther-King-Platz 3, 20146 Hamburg, Germany

ABSTRACT: The shark-like rays (Rhinopristiformes) are among the most threatened species of cartilaginous fishes. The guitarfishes (Rhinobatidae) are one of 5 families in the order, with 62% of species assessed as Vulnerable or higher by the International Union for the Conservation of Nature (IUCN). Species-specific fisheries and conservation efforts have been limited, however, due to unresolved taxonomic issues and poor species descriptions. Presently, there are 3 described species of *Rhinobatos* from the southwestern Indian Ocean (SWIO): *R. austini*, *R. holcorhynchus*, and *R. nudidorsalis*. These 3 species have been mistaken for one another and are assessed as Data Deficient by the IUCN. Since the descriptions of *R. austini* and *R. nudidorsalis*, additional specimens have become available and a rediagnosis of these 3 species is required to clarify their taxonomic status. In the present study, morphometrics from 4 additional congener Indian Ocean species of *Rhinobatos* assessed by the IUCN were analyzed and serve as comparative material. In addition to a traditional morphological analysis, morphometrics from all 7 species were analyzed using a principal component analysis (PCA) and linear discriminant analysis (LDA). Results show distinct clusters for the SWIO *Rhinobatos* and indicate the nasal region is effective in differentiating species. *R. austini*, *R. holcorhynchus*, and *R. nudidorsalis* are confirmed as distinct species and are rediagnosed based on new material. These rediagnoses provide taxonomic clarity for SWIO *Rhinobatos* and will aid in species-specific identification, leading to improvements in conservation and fisheries monitoring and management.

KEY WORDS: Chondrichthyes · Elasmobranchii · Shovelnose rays · Taxonomy · Morphology · Data Deficient

1. INTRODUCTION

The shark-like rays (order Rhinopristiformes) are found worldwide in the tropical, sub-tropical, and warm temperate waters of the Atlantic, Pacific, and Indian oceans. There are currently 5 families in this order (Last et al. 2016): Rhinidae (wedgefishes), Glaucostegidae (giant guitarfishes), Rhinobatidae (guitarfishes), Pristidae (sawfishes), and Trygonorrhinidae (banjo guitarfishes). Species in this order can be difficult to distinguish from one another and are often targeted in fisheries for both their meat and fins (Jabado 2018). Over the last few decades, the increasing demand for shark and ray products has also resulted in intense fishing pressures that are unregulated in many areas (Jabado et al. 2017). As a result, they are among the most threatened groups globally and of high conservation concern (Dulvy et al. 2014, 2021a, Moore 2017, Jabado 2018, Kyne et al. 2020).

*Corresponding author: rachelmaitchison@gmail.com

© The authors and photo licensors 2024. Open Access under Creative Commons by Attribution Licence. Use, distribution and reproduction are unrestricted. Authors and original publication must be credited.

Publisher: Inter-Research · www.int-res.com

Taxonomic issues, including misidentification and unidentified species, can compound conservation and management efforts (Johri et al. 2020). The limited catch information available for batoids is particularly problematic because it contains several misidentifications, many undescribed species that are not recognized in fishery statistics and requires species redescriptions to build confidence in existing fishery data (Simpfendorfer et al. 2011, Last et al. 2016). Poorly understood species distributions and inconsistent species identifications can also hinder status assessments and proper fishery management.

The family Rhinobatidae Bonaparte, 1835 has undergone major taxonomic revisions over the last decade to try to address conservation concerns: Rhinobatidae previously consisted of 7 genera (one of which was highly questionable) and about 48 species (5 of which questionably valid) (Weigmann 2016). After the revision by Last et al. (2016), a new order and family were described and the Rhinobatidae was revised to contain 37 species across 3 genera: *Acroteriobatus* Giltay, 1928, *Pseudobatos* Last, Séret & Naylor, 2016, and *Rhinobatos* Linck, 1790, with 10, 9, and 18 species, respectively. Of these 37 species, 23 (62%) are assessed as Vulnerable or higher (Vulnerable, Endangered, or Critically Endangered) by the International Union for the Conservation of Nature (IUCN). The remaining 14 species are either assessed as Near Threatened (4), Least Concern (3), Data Deficient (5) or Not Evaluated (2). The largest genus in the family, *Rhinobatos*, currently comprises 18 species, two-thirds of which are assessed as Vulnerable or higher (12 species), with 3 species assessed as Near Threatened (1) or Least Concern (2), and 3 species as Data Deficient. All 3 Data Deficient species are found in the southwestern Indian Ocean (SWIO): *R. austini* Ebert & Gon, 2017, *R. holcorhynchus* Norman, 1922, and *R. nudidorsalis* Last, Compagno & Nakaya, 2004.

These 3 species are often misidentified for one another, limiting efforts to investigate their biology and distribution. The description of *R. holcorhynchus* was brief by contemporary standards, and as a result this species was often misidentified with *R. austini* prior to the latter species being recognized as distinct (Ebert & Gon 2017). In addition, *R. nudidorsalis* was described based on a single specimen that was caught near the Mascarene Ridge and may have also been previously misidentified as *R. holcorhynchus* (Last et al. 2004). Since the description of *R. austini* and *R. nudidorsalis*, additional specimens have become available, prompting rediagnosis of these species to clarify their taxonomic status. Resolution of the taxonomic status of these 3 SWIO species will be important for collecting future data for fishery statistics and developing conservation policy.

2. MATERIALS AND METHODS

Morphometric measurements followed the current standard for the Rhinobatidae developed by Last et al. (2004), (2016), (2019). Sixty-three morphological characters were measured to the nearest 0.1 mm on preserved museum specimens identified as *Rhinobatos austini*, *R. holcorhynchus*, and *R. nudidorsalis* from the SWIO. Additional morphometrics were analyzed from preserved specimens of 3 congeners from the western Indian Ocean (WIO), defined as Food and Agriculture Organization of the United Nations (FAO) Fishing Area 51 (Ebert 2013): *R. annandalei* Norman, 1926, *R. lionotus* Norman, 1926, and *R. punctifer* Compagno & Randall, 1987, as well as the recently described *R. ranongensis* Last, Séret & Naylor, 2019 from the northeastern Indian Ocean. Three of the congeners (*R. annandalei*, *R. lionotus*, and *R. punctifer*) were recently redescribed together with the description of a fourth congener — new species, *R. ranongensis* (Last et al. 2019). In addition, all 4 congeners have been recently assessed by the IUCN making them useful comparative material for contextualizing the 3 Data Deficient species (Ebert et al. 2017, Dulvy et al. 2021b,c,d).

Meristics, including nasal lamellae, tooth rows, vertebral, and fin radial counts were also taken. Two facing folds and the slice of raphe between them were considered a nasal lamella so that nasal lamellae could be counted in the posterior half of the nasal capsule following standard methodology in other taxonomic papers on guitarfishes to ensure comparability (e.g. Last et al. 2004, 2006, 2014, 2016, 2019, Ebert & Gon 2017, Weigmann et al. 2021). Although some authors consider each single fold as a lamella (see e.g. Ferrando et al. 2017), this concept has rarely been used in taxonomic publications, limiting comparability. Rosettes were not removed from the capsule to perform lamellar counts in order to avoid damage to the museum specimens, but careful cleaning and microscopic assistance were employed to ensure accurate counts. Pectoral and pelvic fin radial counts, as well as vertebral counts, were taken from radiographs of 10 individuals (*R. austini*: SAIAB 75223, SAIAB 193574, SAIAB 186420, SAM 37223; *R. holcorhynchus*: BMNH 1922.1.13.18, SAIAB 11144; *R. nudidorsalis*: HUMZ 81478, ZMH 25548, SAIAB 84016, SAIAB 84037). Additional radiographs were taken of the holotype of *R. natalensis* (ANSP 53041),

a junior synonym of *R. holcorhynchus* (Ebert & Gon 2017, Ebert et al. 2021), and a photograph of a fresh *R. holcorhynchus* was evaluated; morphometrics for these individuals were not taken.

To evaluate the morphological differences between the 7 species of *Rhinobatos* from the Indian Ocean, a principal component analysis (PCA) and a linear discriminant analysis (LDA) were performed. In a PCA, component axes maximize the variance and the class of each data point is not considered. In an LDA, component axes are maximized for class-separation while minimizing overlap between classes, all while taking into account which class (species) each data point belongs to. When classes (species) are very similar, a PCA may not show as much separation and should be used in conjunction with an LDA.

Both analyses were performed on the percent total length (% TL) of morphological characters for all 7 Indian Ocean *Rhinobatos*. Two additional LDAs were performed on the % TL of 12 characters related to nasal morphology, following Rutledge (2019). The % TL of each character was used to align with the results of traditional morphological analysis and account for differences in TL, allowing congeners to be compared based on body proportions. The primary loadings for the multivariate statistics were determined based on the characters with the largest positive or smallest negative values, defined by a noticeable drop-off in values, for PC1, PC2, LD1 and LD2 (e.g. loading values for PC1 decreased in ~0.05 intervals except for the 2 largest positive values, which had a difference of 0.1).

Analyses were performed using the packages 'caret', 'Hmisc', 'factoextra', 'MASS', 'tidyverse', and 'vegan' in R v 4.2.0 (R Core Team 2021). Plots were created using the R function 'ggplot' from the 'ggplot2' package and 'ggbiplot'.

3. RESULTS

3.1. Statistical results

The PCA performed on the % TL of measurements for the 7 *Rhinobatos* species from the Indian Ocean showed some separation between species with some clustering within species (Fig. 1). Although there was overlap between *R. lionotus* and the following species — *R. austini*, *R. holcorhynchus*, *R. nudidorsalis*, and *R. ranongensis*, the 3 SWIO *Rhinobatos* species did not overlap with each other. PC1 explained 27% of variance while PC2 explained 15% of variance. PC1 loaded mostly with characters related to body size such as ventral head length and interdorsal space, and mouth width. PC2 primarily loaded with characters related to first dorsal fin morphology and presocket snout length (Table S1 in the Supplement at www.int-res.com/articles/suppl/n053p067_supp.pdf).

The LDA performed on the % TL of measurements for the 7 Indian Ocean *Rhinobatos* species showed separation between every species except *R. austini* and *R. holcorhynchus* and some tight clustering within species (Fig. 2). LD1 primarily loaded with posterior nasal flap width, second dorsal fin inner margin length, and maximum body depth. LD2 pri-

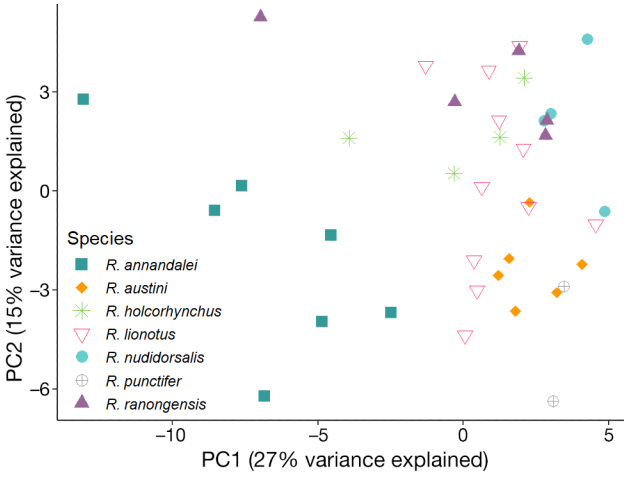

Fig. 1. Principal component analysis of 7 Indian Ocean *Rhinobatos* based on the percent total length of 62 morphological characters used to describe guitarfish

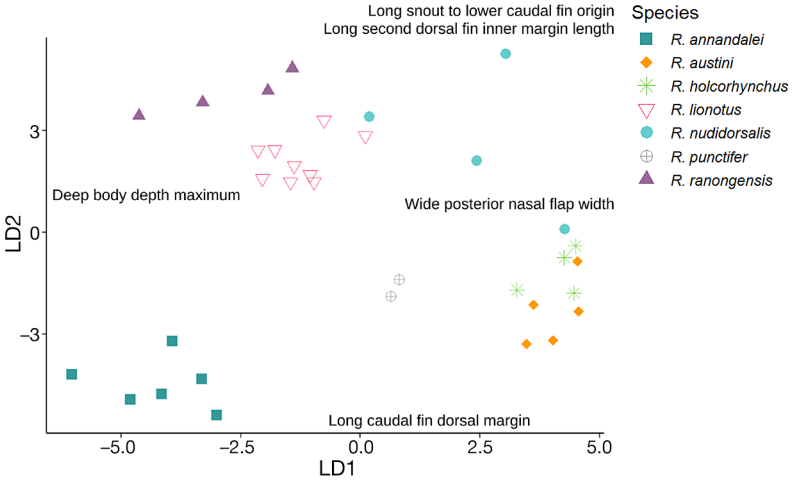

Fig. 2. Linear discriminant analysis of 7 Indian Ocean *Rhinobatos* based on the percent total length of 62 morphological characters used to describe guitarfish

marily loaded with caudal fin dorsal margin and snout to lower caudal fin origin (Table S2).

The LDA performed on the % TL of nasal characters for the 7 Indian Ocean *Rhinobatos* showed separation between every species except *R. lionotus* and *R. ranongensis*, and clustering within species (Fig. 3). LD1 primarily loaded with nostril length, distance from nostril to disc margin, distance between anterior nasal flaps, and posterior nasal flap width. LD2 primarily loaded with distance from nostril to disc margin and distance across anterior nasal apertures (Table S3). The LDA performed on the % TL of nasal characters for the 3 SWIO *Rhinobatos* showed clear separation between species with clustering within species (Fig. 4). LD1 primarily loaded with nostril length, distance from nostril to disc margin, anterior nasal flap base length and posterolateral nasal flap TL. LD2 primarily loaded with nostril length and distance from nostril to disc margin (Table S4).

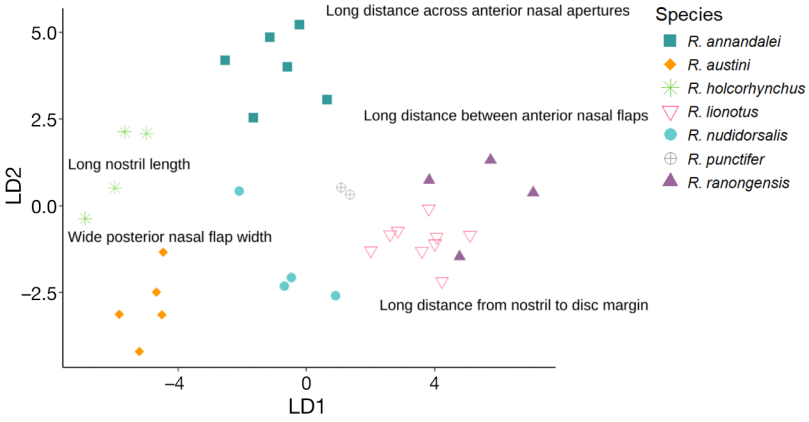

Fig. 3. Linear discriminant analysis based on the percent total length of 12 morphological characters related to nasal morphology for 7 Indian Ocean *Rhinobatos*

3.2. Systematics

3.2.1. *Rhinobatos austini* Ebert & Gon, 2017

Austin's guitarfish (Figs. 5–9; Tables 1–3, Table S5)
Rhinobatus annulatus (natal form): Wallace (1967), p. 27, Fig. 15 (in part); Compagno et al. (1989), p. 78 (in part); Heemstra & Heemstra (2004), p. 78. *Rhinobatos holcorhynchus*: Séret et al. (2016), p. 98, Fig. 10.20 (in part, illustration is of *R. austini*). *Rhinobatos austini*: Ebert & Gon (2017), p. 205, Figs. 1–6; Ebert et al. (2021), p. 76; Séret (2022), p. 373; Séret & Carvalho (2022), p. 569, Plate 59.

Material examined. Six specimens. (1) Holotype, SAIAB 75223, female 1150 mm TL, near Port Shepstone, KwaZulu-Natal Province, South Africa, 30° 50′ S, 30° 29′ E, captured while shore angling from beach by B. Mann, Oceanographic Research Institute, Durban, March 2004; (2) paratype, SAIAB 193574, female 1130 mm TL, Orange Rocks, South Coast, KwaZulu-Natal Province, South Africa, 30° 49.74′ S, 30° 24.2′ E, captured while shore angling from beach by L. Allison, Oceanographic Research Institute (formerly ORI 229-7/11), May 2011; (3) paratype, SAIAB 186420, female 1115 mm TL, off Umlalazi, KwaZulu-Natal Province, South Africa, 29° 06.642′ S, 32° 07.324′ E, ACEP trawl 4-1, FRS Algoa, bottom trawl, 128 m, collected by S. Fennessy, Oceanographic Research Institute, 21 March 2010; (4) paratype, SAM 37223, female 888 mm TL, north of Bazaruto Island, central Mozambique, 20° 54′ 48″ S, 35° 44′ 38″ E, bottom trawl, depth 107 m, 18 October 2007. (5) SAIAB 11125, female 1160 mm TL, Durban, KwaZulu-Natal Province, South Africa. (6) SAIAB 235767, male 815 mm TL, south of Bazaruto, Mozambique, 23° 5′ 45″ S, 35° 43′ 16″ E, bottom trawl, 14 August 2002.

Diagnosis. A large species of *Rhinobatos* (attaining at least 1160 mm TL) distinguished by the following combination of characters: snout bluntly pointed, length 3.1–4.0 times interorbital width; ventral head length 25.9–27.4 % TL; presocket snout length 12.7–

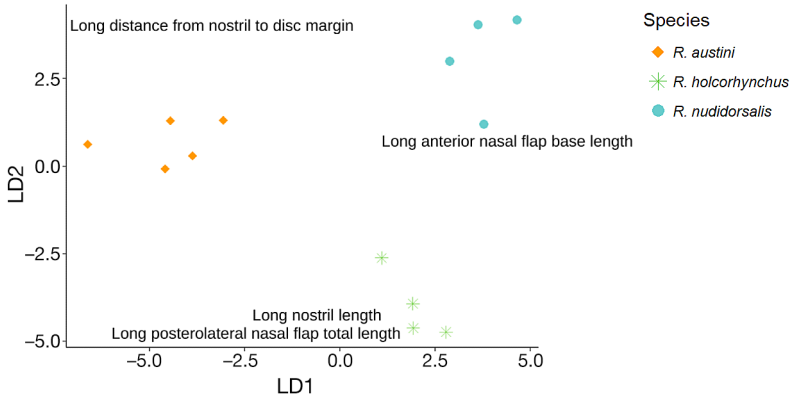

Fig. 4. Linear discriminant analysis based on the percent total length of 12 morphological characters related to nasal morphology for the 3 southwestern Indian Ocean *Rhinobatos*

Fig. 5. Dorsal views of *Rhinobatos*. (A) *R. austini*, male, 815 mm total length (TL), preserved (SAIAB 235767). (B) *R. holcorhynchus*, male, 697 mm TL, preserved (BMNH 1922.1.13.18). (C) *R. nudidorsalis*, male, 673 mm TL (SAIAB 84016), preserved. Scale bars = 5 cm. Photographs courtesy (A) © David Ebert, (B) © Harry Taylor, (C) © Marsha Englebrecht

15.1% TL; nostrils diagonal, their length 1.7–1.9 times internarial distance; mouth width 5.4–6.2% TL; anterior nasal flaps inserted into internarial space; posterior nasal flaps lobe-like, inner edges nearly reaching the innermost margin of the nostril; spiracles fairly large and bean-shaped; gill openings sinusoidal; distance between fifth gill slits 3.8–4.3 times internarial distance; post-scapular sensory canal indistinct, terminating near pectoral fin insertions; male with orbital thorns 12–13 (left), irregularly spaced of various sizes, extending in a semi-circle pattern from anterior eye socket to inner margin of spiracle, midback thorns ~40–45, irregularly spaced to first dorsal fin origin, with 1–3 thorns irregularly scattered between dorsal fins; dorsal fins moderately tall, height of first 7.9–9.4% TL; body depth at second dorsal fin origin 2.6–3.2% TL; tooth row counts 80–93 in upper and lower jaws; 61–64 nasal lamellae; 193–198 total (synarcual and free) vertebral segments, 27–31 monospondylous precaudal centra, 41–42 diplosondylous caudal centra, monospondylous to diplosondylous centra transition posterior to pelvic fin girdle; dorsal surface light to medium or yellowish brown with a distinctive pattern of

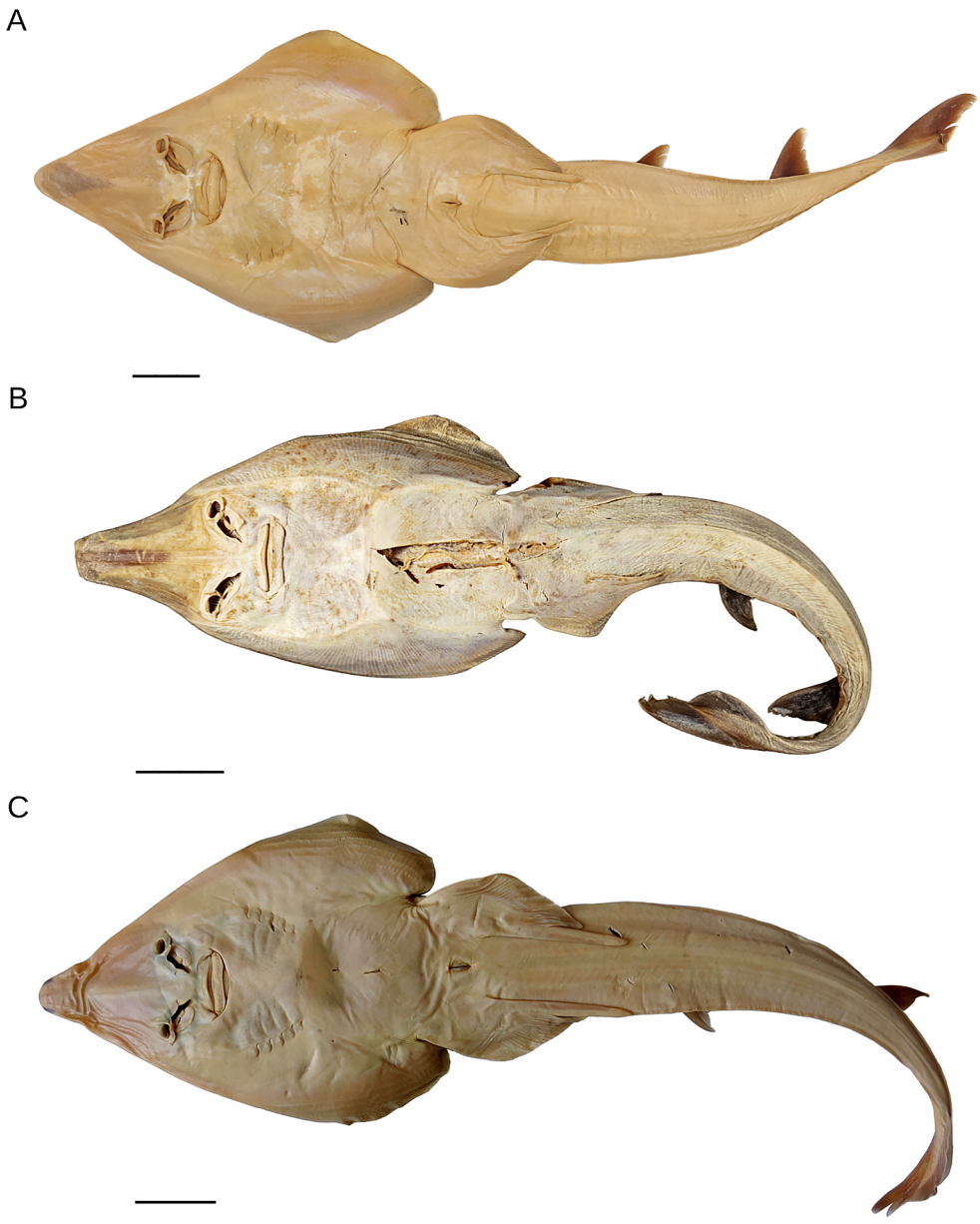

Fig. 6. Ventral views of *Rhinobatos*. (A) *R. austini*, male, 815 mm total length (TL), preserved (SAIAB 235767). (B) *R. holcorhynchus*, male, 697 mm TL, preserved (BMNH 1922.1.13.18). (C) *R. nudidorsalis,* male, 673 mm TL (SAIAB 84016), preserved. Scale bars = 5 cm. Photographs courtesy (A) © David Ebert, (B) © Lucie Goodayle, (C) © Marsha Englebrecht

Fig. 7. Ventral views of the snout and oronasal region of *Rhinobatos*. (A) *R. austini*, male, 815 mm total length (TL), preserved (SAIAB 235767). (B) *R. Holcorhynchus*, male, 697 mm TL, preserved (BMNH 1922.1.13.18). (C) *R. nudidorsalis*, male, 695 mm TL (SAIAB 84037), preserved. Scale bars = 2 cm. Photographs courtesy (A) © David Ebert, (B) © Harry Taylor, (C) © Marsha Englebrecht

paired spots of various sizes, sometimes forming darker bands; ventral surface mostly white except for teardrop-shaped dark blotch extending from the rostral tip to about midpoint anterior to upper mouth.

Distribution. *R. austini* broadly overlaps with *R. holcorhynchus* from Port Shepstone, southern KwaZulu-Natal Province, South Africa to north of Bazaruto Island, central Mozambique. Both species may also co-occur

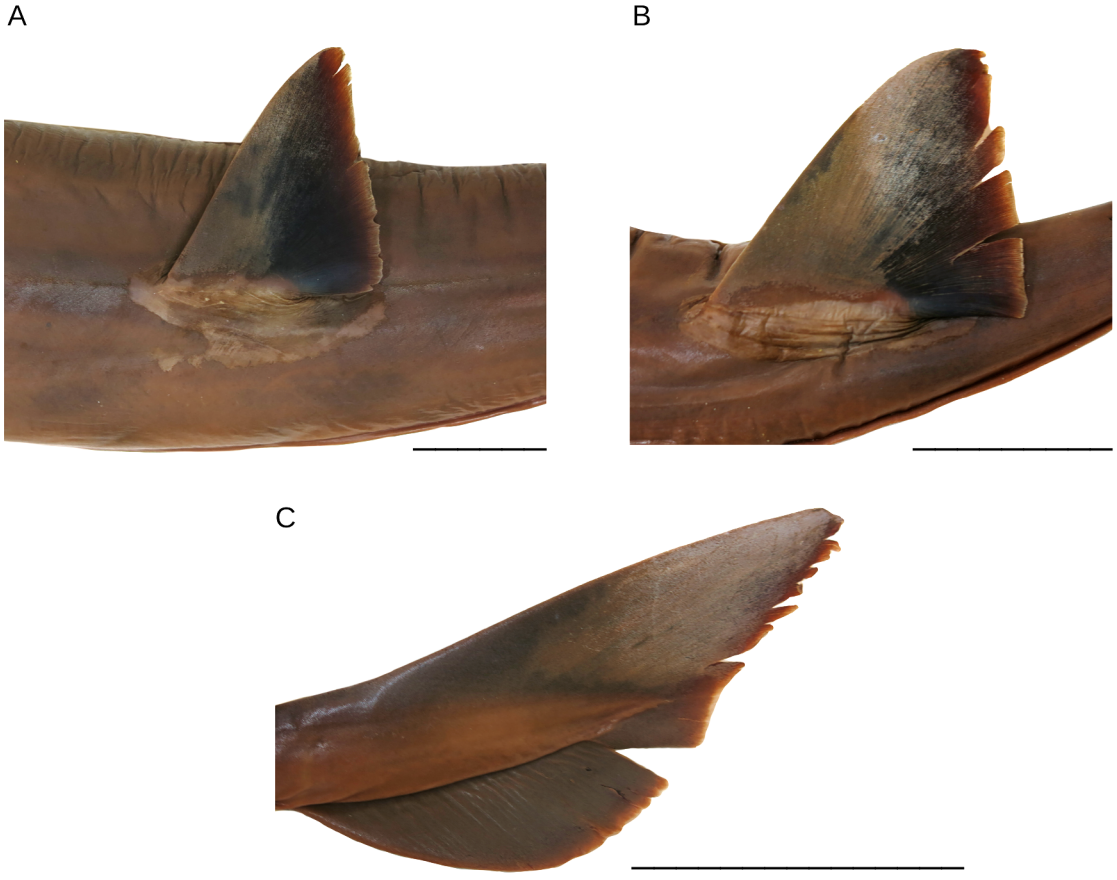

Fig. 8. *Rhinobatos austini*, female, 1160 mm total length (TL) (SAIAB 11125), preserved. Lateral views of (A) the first dorsal fin, (B) the second dorsal fin, (C) the caudal fin. Scale bars = 5 cm. Photographs courtesy © David Ebert

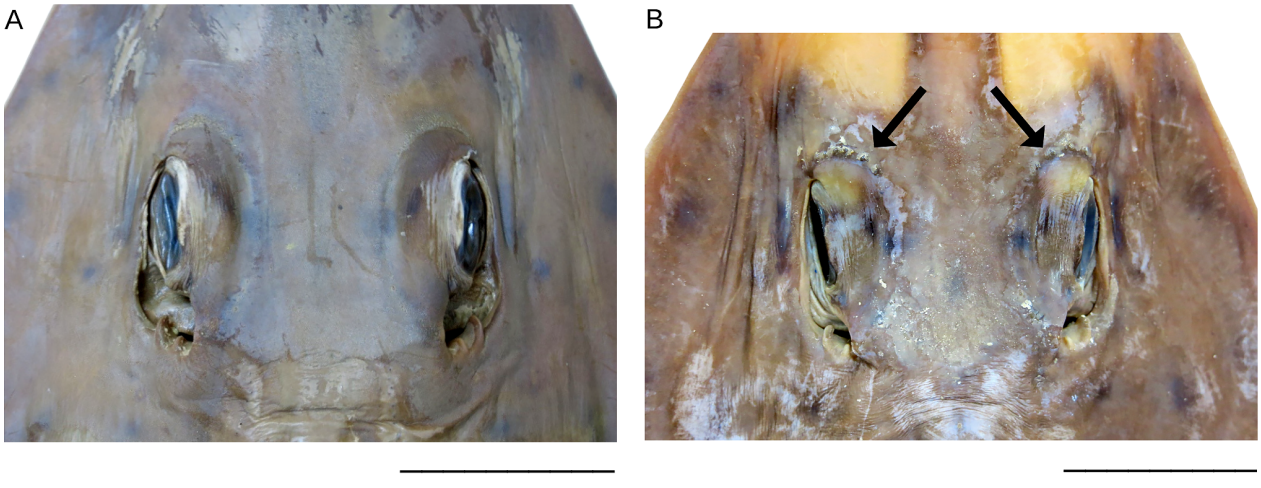

Fig. 9. Orbital region of *Rhinobatos austini*. (A) Preserved female (SAIAB 11125), 1160 mm total length (TL), without orbital thorns. (B) Preserved male non-type (SAIAB 235767), 815 mm TL, orbital thorns denoted by arrows. Scale bars = 5 cm. Photographs courtesy © David Ebert

Table 1. Morphometric data for *Rhinobatos austini*, *R. holcorhynchus*, and *R. nudidorsalis*. TL: total length

	R. austini 6 specimens		*R. holcorhynchus* 4 specimens		*R. nudidorsalis* 4 specimens	
	Min.	Max.	Min.	Max.	Min.	Max.
TL (mm)	815	1160	306	697	501	740
Disc width–max. (% TL)	31.4	34.9	30.3	32.7	29.1	32.6
Disc length (% TL)	41.1	43.8	40.9	42.8	39.1	41.5
Head length–dorsal (% TL)	26.6	38.3	28.5	30.7	19.9	27.2
Head length–ventral (% TL)	25.9	27.4	27.7	28.2	25.5	27.3
Snout length–presocket (% TL)	12.7	15.1	15.2	16.0	14.6	15.2
Snout to first dorsal-fin origin (% TL)	56.1	58.2	56.0	58.2	57.4	58.1
Snout to second dorsal-fin origin (% TL)	73.0	75.2	73.4	75.2	74.3	75.3
Snout to upper caudal-fin origin (% TL)	84.3	87.6	85.0	86.6	86.0	87.2
Snout to lower caudal-fin origin (% TL)	86.2	88.5	87.5	88.7	88.1	89.2
Snout to pelvic-fin origin (% TL)	37.8	39.3	39.0	39.8	37.2	38.6
Snout to anterior vent (% TL)	41.4	43.4	40.2	43.1	40.0	40.4
Pelvic-fin insertion to first dorsal-fin origin (% TL)	9.5	20.3	9.8	11.4	11.4	14.1
Interdorsal space (% TL)	11.9	12.5	12.3	13.6	12.4	13.4
Caudal peduncle length (dorsal) (% TL)	6.6	7.9	7.5	8.2	6.9	12.4
Disc width–anterior orbit (% TL)	15.2	19.7	15.5	18.0	15.8	18.1
Body width–pelvic insertion (% TL)	9.0	16.0	7.4	13.1	8.9	10.8
Body width–first dorsal-fin origin (% TL)	8.4	10.4	7.0	9.8	8.8	10.5
Body width–second dorsal-fin origin (% TL)	4.6	5.6	3.3	5.7	5.0	5.4
Body depth–maximum (% TL)	4.9	6.7	4.0	4.9	3.4	4.7
Body depth–pelvic-fin insertion (% TL)	4.7	5.3	3.9	4.3	3.9	4.3
Body depth–first dorsal-fin origin (% TL)	3.8	4.7	3.6	4.5	3.5	4.6
Body depth–second dorsal-fin origin (% TL)	2.6	3.2	2.3	2.5	2.2	2.3
Orbit diameter (% TL)	3.2	4.7	3.9	5.2	3.6	4.5
Spiracle length (% TL)	2.0	2.8	1.8	2.9	1.8	2.2
Orbit and spiracle length (% TL)	4.6	5.8	5.6	6.9	4.2	5.2
Interorbital width (% TL)	3.4	4.1	3.5	4.2	2.9	3.3
Interspiracle width (% TL)	5.1	5.8	5.2	6.5	4.9	5.8
Pelvic fin–length (% TL)	14.4	15.5	14.0	15.0	14.8	16.6
Pelvic fin–anterior margin length (% TL)	7.0	9.3	7.0	8.2	7.3	9.5
Pelvic fin–width (% TL)	4.8	6.7	5.6	8.4	5.8	6.5
Pelvic fin–base length (% TL)	7.7	9.6	7.1	8.8	7.4	9.5
Pelvic fin–inner margin length (% TL)	6.0	8.1	5.6	7.2	6.9	8.8
First dorsal fin–length (% TL)	6.1	6.8	5.3	6.8	6.2	7.0
First dorsal fin–anterior margin length (% TL)	8.9	10.4	8.7	10.5	8.9	9.6
First dorsal fin–height (% TL)	7.9	9.4	6.7	8.4	7.0	7.9
First dorsal fin–base length (% TL)	3.8	4.6	3.6	4.3	3.6	4.6
First dorsal fin–inner margin length (% TL)	1.9	2.6	2.4	3.0	2.3	2.7
Second dorsal fin–length (% TL)	6.5	7.0	5.7	6.6	6.0	7.0
Second dorsal fin–anterior margin length (% TL)	4.8	10.1	7.9	9.3	8.2	9.3
Second dorsal fin–height (% TL)	3.9	7.8	6.5	7.5	6.1	7.0
Second dorsal fin–base length (% TL)	4.3	4.6	3.6	4.4	3.9	4.9
Second dorsal fin–inner margin length (% TL)	1.8	2.2	2.0	2.6	2.3	2.6
Caudal fin–dorsal margin (% TL)	12.8	14.6	11.9	15.0	11.9	13.5
Caudal fin–preventral margin (% TL)	4.7	7.0	5.4	7.2	5.9	6.9
Preoral length (% TL)	15.0	18.0	18.0	18.7	17.2	19.1
Mouth width (% TL)	5.4	6.2	6.0	7.2	5.0	5.3
Prenarial length (% TL)	12.0	13.9	13.6	14.1	13.2	14.2
Nostril length (% TL)	4.1	4.7	4.4	4.9	3.8	4.5
Anterior nasal aperture–width (% TL)	1.2	2.0	1.5	1.8	1.2	1.5
Anterior nasal flap–base length (% TL)	2.6	3.0	2.8	3.3	2.7	3.3
Anterior nasal flap–width (% TL)	1.3	2.5	1.4	2.0	1.5	2.1
Posterolateral nasal flap–total length (% TL)	2.8	3.6	3.1	3.7	2.9	3.6
Posterolateral nasal flap–width (%TL)	0.4	1.3	0.5	1.0	0.7	0.9
Posterior nasal flap–base length (% TL)	2.7	3.4	2.6	3.5	2.6	2.9
Posterior nasal flap–width (% TL)	1.3	1.9	1.0	2.0	1.0	1.3
Distance across anterior nasal apertures (% TL)	6.7	9.2	9.3	10.5	8.4	9.3
Distance between anterior nasal flaps (% TL)	2.3	3.4	2.4	3.3	1.9	2.9
Internarial distance–minimum width (% TL)	2.3	2.7	2.3	3.3	2.2	2.5
Distance from nostril to disc margin (% TL)	3.0	4.3	2.0	3.6	3.1	3.6
Third gill opening–width (% TL)	1.4	1.6	0.9	2.0	1.2	1.4
Distance between first gill openings (% TL)	12.0	13.9	11.6	13.7	10.6	12.2
Distance between fifth gill openings (%TL)	9.3	10.4	8.7	12.7	7.5	8.0
Angle before eyes (°)	57.5	67.9	55.7	59.8	55.7	65.0

Table 2. Meristic data for *Rhinobatos austini*, *R. holcorhynchus*, and *R. nudidorsalis*

	R. austini Austin's guitarfish	*R. holcorhynchus* Slender guitarfish	*R. nudidorsalis* Bareback guitarfish
Tooth rows in upper jaw (n)	80–93	63–73	78–79
Tooth rows in lower jaw (n)		78	
Nasal lamellae (n)	61–64	68–75	45–55
Propterygial pectoral radials (n)	31–33	32–33	29–30
Mesopterygial pectoral radials (n)	8	8	7–9
Neopterygial pectoral radials (n)	1–2	1–2	2
Metapterygium pectoral radials (n)	27–28	24–29	27–28
Total pectoral radials (n)	67–71	66–72	68
Total pelvic radials (n)	28–29	26–29	29
Total vertebral segments (n)	193–198	199–209	189–201
Post synarcural centra (n)	177–181	185–194	183–187
Precaudal centra (n)	135–140	147–156	153–155
Synarcural segments (n)	16–18	14–15	14–16
Monospondylous precaudal centra (n)	27–31	39–52	26–36
Diplospondylous precaudal centra (n)	105–110	104–110	109–120
Diplospondylous caudal centra (n)	41–42	37–38	30–40

Table 3. Summary of diagnostic characters for *Rhinobatos austini*, *R. holcorhynchus*, and *R. nudidorsalis*. TL: total length

	R. austini Austin's guitarfish	*R. holcorhynchus* Slender guitarfish	*R. nudidorsalis* Bareback guitarfish
Max. TL (mm)	1160	697	740
Depth range (m)	<1–107	75–254	87–219
Morphometrics			
Head length–ventral (% TL)	25.9–27.4	27.7–28.2	25.5–27.3
Snout length–presocket (% TL)	12.7–15.1	15.2–16.0	14.6–15.2
Snout to pelvic-fin origin (% TL)	37.8–39.3	39.0–39.8	37.2–38.6
Body depth–second dorsal-fin origin (% TL)	2.6–3.2	3.3–5.7	2.2–2.3
Mouth width (% TL)	5.4–6.2	6.0–7.2	5.0–5.3
Distance across anterior nasal apertures (% TL)	6.7–9.2	9.3–10.5	8.4–9.3
Meristics			
Nasal lamellae (n)	61–64	68–75	45–55
Monospondylous centra (n)	27–31	39–52	34–36
Diplospondylous caudal centra (n)	41–42	37–38	30–40
Coloration			
Dorsal surface	Light to medium or yellowish brown with a pattern of paired dark brown spots of varying sizes, sometimes forming transverse bands	Plain olive green to brown	Light to medium yellowish brown, may have a variable spot pattern
Ventral surface	Mostly white with a teardrop-shaped dark blotch on snout tip	Mostly white with a teardrop-shaped dark blotch on snout tip	Mostly white with a black line along each side of snout
Dorsal surface thorns			
Orbital thorns (n)	12–13 (male)	5–13	0
Scapular thorns (n)	0	2–3	0
Midback thorns (n)	40–45 (male)	27–40	0
Interdorsal thorns (n)	1–3 (male)	6–18	0
Post dorsal thorns (n)	0	3–9	0
Nasal morphology			
Anterior nasal flaps	Extend into internarial space	Extend to inner edge of nostril	Extend into internarial space

along the coast of Madagascar (Fricke et al. 2018). However, *R. austini* appears to be a more coastal species than *R. holcorhynchus* since it was mostly caught from shore and in bottom trawls less than 107 m deep (Ebert & Gon 2017). It may also have a wider distribution than *R. holcorhynchus* (Ebert & Gon 2017).

Remarks. Most proportional body measurements reported here were either very similar to or the same as those reported by Ebert & Gon (2017), which was based solely on female *R. austini* specimens. Most of the differences were apparently due to describing the first male specimen of this species. *R austini* seems to exhibit several differences in body proportions between the male and females including a longer presocket snout length (15.1 vs. 12.7–14.6% TL) and shorter spiracle length (2.0 vs. 2.3–2.8% TL). The male specimen also possesses thorns on the dorsal surface while the females do not. Currently, no other instances of sexual dimorphism with respect to dorsal surface thorns have been reported in any species of *Rhinobatos* from the Indian Ocean. Additional male specimens are needed to confirm the extent of this variability both within males and between males and females.

Coloration in preserved specimens appears to change based on length of preservation. Compared to fresh specimens (see Fig. 6 of Ebert & Gon 2017), the dorsal surface and spots darken after preservation, but the spot pattern and banding is otherwise similar. After 17 yr of preservation, the dorsal surface darkened further with some spots slightly faded. Ventral surface coloration is similar to specimens prior to preservation except the outer portion of pectoral and pelvic fins darkened slightly.

R. austini is most similar to *R. holcorhynchus*, and the 2 species are frequently misidentified since both species possess a teardrop-shaped dark blotch on the ventral surface of the snout (Séret et al. 2016, Ebert & Gon 2017). *R. holcorhynchus* was long thought to be the only *Rhinobatos* species in the SWIO to have a teardrop-shaped dark blotch on the ventral snout surface. The proportional size of each morphological character relative to body length is also similar for both species; however, *R. austini* can be distinguished by a proportionally shorter presocket snout length (12.7–15.1 vs. 15.2–16.0% TL), snout to pelvic fin origin length (37.8–39.3 vs. 39.5–39.8% TL), orbit and spiracle length (4.6–5.8 vs. 6.4–6.9% TL), and distance across anterior nasal apertures (6.7–9.2 vs. 9.3–10.5% TL). *R. austini* is also proportionally deeper at the second dorsal fin origin (2.6–3.2 vs. 2.3–2.4% TL) and has a proportionally longer second dorsal fin base length (4.3–4.6 vs. 3.6–4.1% TL) than *R. holcorhynchus*. In addition, the anterior nasal flaps of *R. austini* extend into internarial space while the anterior nasal flaps of *R. holcorhynchus* extend to the inner edge of the nostril but not into internarial space. In terms of meristics, *R. austini* has fewer nasal lamellae than *R. holcorhynchus* (61–64 vs. 68–75).

3.2.2. *Rhinobatos holcorhynchus* Norman, 1922

Slender guitarfish (Figs. 5–7, 10–12, Tables 1–3, Table S6) *Rhinobatus holcorhynchus*: von Bonde & Swart (1923), p. 3; Barnard (1925), p. 61, Fig. 9c, Plate 3; Norman (1922), p. 318; Norman (1926), p. 957, Fig. 10; Barnard (1927), p. 1014; Fowler (1941), p. 307; Barnard (1959), p. 22; Wallace (1967), p. 18, Figs. 9 & 11. *Rhinobatus natalensis*: Fowler (1925), p. 195, Fig. 1. *Rhinobatus schlegeli*: Smith (1949) p. 64, Fig. 64; Smith (1961), p. 64, Fig. 64; Smith (1965), p. 64, Fig. 64. *Rhinobatos holcorhynchus*: Compagno (1986), p.130, Fig. 27.4; Compagno et al. (1989), p. 78; Compagno (1999), p. 116; Heemstra & Heemstra (2004), p. 78; NPOA (2013), p. 57; da Silva et al. (2015), p. 247; Ebert & van Hees (2015), p. 146; Last et al. (2016a), p. 470; Séret et al. (2016), p. 98, Fig. 10.20 (in part, illustration is of *R. austini*); Weigmann (2016), p. 922; Ebert et al. (2021), p. 77; Séret (2022), p. 373; Séret & Carvalho (2022), p. 570, Plate 59.

Material examined. Four specimens. (1) Holotype, BMNH 1922.1.13.18, subadult male 711 mm TL (fresh), 697 mm TL (preserved), captured at 73 m depth, near Zululand Coast, South Africa; (2) SAIAB 11146 (formerly ORI B 836), immature male 306 mm TL, captured during continental slope trawl near Umhloti and Nonoti rivers, ~74–140 m depth, north-

Fig. 10. *Rhinobatos holcorhynchus*, female, fresh, specimen not retained (Richards Bay, trawl, 127 m depth, 28° 42.021′ S, 32° 24.018′ E–28° 40.913′ S, 32° 24.582′ E, 20 March 2010). Scale bar = 5 cm. Photograph courtesy © Sean Fennessy

Fig. 11. *Rhinobatos holcorhynchus*, male, 440 mm total length (TL) (SAIAB 11144), preserved. Lateral views of (A) the dorsal fins, scale bar = 2 cm; (B) the caudal fin, scale bar = 5 cm. Photographs courtesy © David Ebert

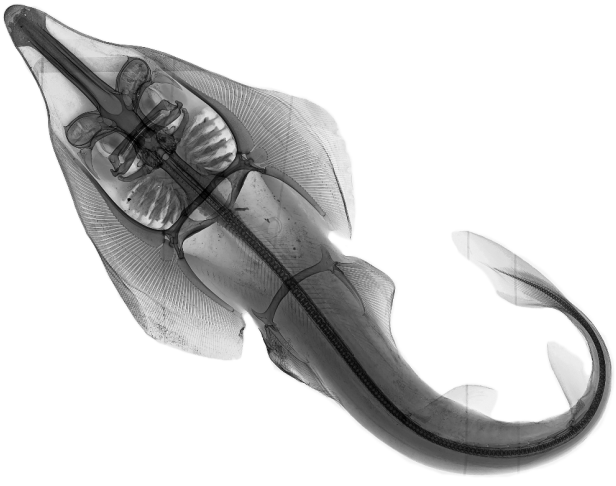

Fig. 12. Radiograph of *Rhinobatos holcorhynchus*, male, 697 mm total length (TL) (BMNH 1922.1.13.18). Courtesy of © James Maclaine and © Chrissy Williams

east of Durban Bluff, KwaZulu-Natal Province, South Africa; (3) SAIAB 11144 (formerly ORI B 797), immature male 440 mm TL, captured during continental slope trawl near Umhloti and Nonoti rivers, ~74–140 m depth, northeast of Durban Bluff, KwaZulu-Natal Province, South Africa; (4) SAIAB 11145 (formerly ORI B 835), immature female 462 mm TL, captured during continental slope trawl near Umhloti and Nonoti rivers, ~74–140 m depth, northeast of Durban Bluff, KwaZulu-Natal Province, South Africa.

Diagnosis. A medium-sized species of *Rhinobatos* (attaining at least 711 mm) distinguished by the following combination of characters: snout bluntly pointed, length 3.8–4.2 times interorbital width; ventral head length 27.7–28.2% TL; presocket snout length 15.2–16.0% TL; nostrils diagonal, their length 1.5–1.8 times internarial distance; mouth width 6.0–7.2% TL; anterior nasal flaps not inserted into internarial space; posterior nasal flaps lobe-like, inner edges nearly reaching the innermost margin of the nostril; spiracles fairly large and teardrop-shaped; gill openings slightly sinusoidal; distance between fifth gill slits 3.6–3.9 times internarial distance; postscapular sensory canal indistinct, terminating near pectoral fin insertions; dorsal surface with 3–10 erupted, 2–3 non-erupted anterior orbital thorns, 2–3 erupted, several non-erupted posterior orbital thorns (left); at least 1 large thorn at spiracle edge with at least 2 thornlets perpendicular to spiracle; 27–40 semi-regularly to irregularly spaced thorns with smaller thornlets along midback; a pair of 2 thorns lateral to midback thorns on pectoral girdle; 6–18 thorns with smaller thornlets between dorsal fins; 3–9 small thorns between second dorsal fin and upper caudal fin origin; dorsal fins relatively tall, height of first 7.4–8.4% TL; body depth at second dorsal fin origin 3.3–5.7% TL; tooth row counts range from 63–73 in upper and lower jaws; 68–75 nasal lamellae; 199–209 total (synarcual and free) vertebral segments, 39–52 monospondylous precaudal centra, 37–38 diplosondylous caudal centra, monospondylous to diplosondylous centra transition posterior to pelvic fin girdle; dorsal surface plain olive green to brown with no patterns, spots, or markings; ventral surface mostly white except for teardrop-shaped dark blotch extending from the rostral tip to about midpoint anterior to upper mouth.

Description. Proportional measurements expressed as a % TL are given for the holotype followed in parentheses by a range for 3 non-types (Table 2). Disc broadly wedge-shaped; bluntly angular anteriorly, angle in front of eyes 57.0° (55.7–59.8°); anterior margin relatively straight near tip (concave after preservation) then becoming straight to pectoral apex; outer pectoral fins broadly rounded becoming narrowly rounded distally; disc length 1.38 (1.31–1.36) times maximum disc width. Pelvic fins fairly

long, base length 1.00 (1.23–1.50) times inner margin length; total length 1.99 (1.70–1.80) times their base length, 2.50 (1.70–2.56) times their width; anterior margin slightly convex anteriorly, pelvic apex broadly rounded, posterior margin almost straight, nearly reaching a rounded point distally. Tail long, tapering weakly; in cross-section rounded dorsally, nearly flat ventrally; length from anterior cloaca 1.49 (1.32–1.41) times precloacal length, 1.43 (1.33–1.42) times disc length, 8.10 (4.35–5.62) times its width at pelvic fin insertion; tail width 1.79 (2.50–3.33) times depth at pelvic-fin insertion, 1.78 (2.14–2.69) times depth at first dorsal fin origin, 1.33 (1.71–2.50) times depth at second dorsal fin origin. Clasper of immature male 4.90–5.23% TL. Dermal fold lateral along tail, originating posterior to pelvic fin rear tips; fold well developed.

Head moderately elongate, ventral length 27.96% TL (27.71–28.18% TL); snout bluntly pointed, preoral length 3.10 (2.50–3.00) times mouth width, 8.05 (5.50–7.18) times internarial distance, 1.34 (1.20–1.53) times caudal fin-dorsal margin, 9.25 (5.00–6.08) times distance from nostril to margin of disc; presocket snout length 2.99 (2.45–2.96) times interspiracular width, 3.73 (3.06–3.94) times orbit diameter, 4.45 (3.77–4.19) times interorbital width; interorbital space broad and very weakly concave; eyes large, elevated slightly but not protruding; orbits moderately small, diameter 2.27 (1.50–2.22) times spiracle length, 1.20 (1.00–1.25) times interorbital distance. Spiracles fairly large and teardrop-shaped; 2 compressed folds on upper posterior margin, innermost fold about two-thirds the length of outer fold, distance between bases of folds slightly less than or equal to the length of inner fold.

Nostrils diagonal with well-developed nasal flaps; anterior aperture width slightly greater than length; nostril length 2.97 (2.50–3.14) times anterior aperture width, 1.59 (1.47–1.54) times anterior nasal flap base length, 2.19 (1.36–1.54) times distance from nostril to disc margin, 1.91 (1.50–1.83) times internarial distance. Anterior nasal flap narrow with slender, slightly curved process; flap base length 2.00 (1.67–1.88) times width at process, 1.87 (1.63–2.14) times anterior aperture width; not inserted into internarial space; distance between insertions of flaps 3.40 (2.87–3.46) in greatest distance across nostrils anteriorly, 0.84 (0.80–1.00) in minimum internarial distance; process of flap over twice as long as wide, narrowing distally to a rounded point, overlapping with posterolateral nasal flap and anterior aperture posterior margin. Posterolateral nasal flap lobe-like, length 5.86 (3.33–5.00) times its width; origin slightly posterior to lateral margin of anterior nasal aperture. Posterior nasal flap lobe-like, base length 3.07 (1.33–2.29) times width, its inner edge nearly reaching the innermost margin of the nostril; width 0.67 (0.88–1.20) times anterior aperture width, 1.89 (1.75–2.33) times posterolateral nasal flap width. Nasal lamellae 68 (71–75).

Mouth width 1.36 (1.27–1.47) times nostril length, 6.65 (6.00–6.93) in precloacal length. Upper jaw nearly straight, upper lip gently arched; lower lip pronounced, separated from oral groove by ridges of strongly corrugated skin; weak lateral grooves around corners of mouth. Teeth small, close-set, arranged in quincunx, crowns rhomboidal; upper and lower jaw teeth similar in size and shape; tooth row counts range from (63–72) in upper and lower jaws. Gill openings slightly sinusoidal, the first 4 more so, the fifth mostly straight; length of third gill slit 2.73 (2.50–5.50) in nostril length, 5.35 (6.50–10.75) in distance between fifth gill slits; distance between first gill slits 1.34 (1.08–1.36) times distance between fifth gill slits; distance between fifth gill slits 3.73 (3.58–3.90) times internarial distance, 1.43 (1.54–1.77) times mouth width, 0.31 (0.34–0.45) of ventral head length.

Dorsal fins relatively tall, triangular; anterior margins slightly convex at base, becoming relatively straight, then broadly curving towards rounded apices; posterior margins slightly convex near tips, then becoming nearly straight; free rear tips rounded, nearly forming right angle; first dorsal fin slightly taller than second, length of first 0.79 (0.81–0.88) times height, its base length 1.63 (1.22–1.73) times inner margin length; second dorsal fin length 0.85 (0.88–0.95) times its height, base length 2.15 (1.38–1.73) times inner margin length. First dorsal fin origin just posterior to pelvic-fin insertion, interspace 0.72 (0.83–0.92) times interdorsal space; interdorsal space 2.01 (1.64–1.90) times second dorsal fin height, 3.47 (2.84–3.45) times first dorsal fin base length, 1.65 (1.59–1.67) times interspace between second dorsal-fin insertion and upper origin of caudal fin, 1.95 (1.26–1.41) times tail width at first dorsal fin origin. Caudal fin relatively small, deep; dorsal caudal margin length 2.49 (2.09–2.20) times preventral margin length.

Dermal denticles close-set, minute, covering entire body and fins. Dorsal surface with 8 (3–10 erupted, 2–3 non-erupted) anterior orbital thorns; several abraded (2–3 erupted, several non-erupted) posterior orbital thorns (left); juveniles with at least 1 large thorn at spiracle edge with at least 2 thornlets perpendicular to spiracle; 27 (27–40) semi-regularly to irregularly spaced thorns with smaller thornlets along midback; a set of 3 (2) thorns lateral to midback

thorns on pectoral girdle; 6 (6–18) thorns with smaller thornlets between dorsal fins; 0 (3–9 small) thorns between second dorsal fin and upper caudal fin origin. Post-scapular sensory canal indistinct, terminating near pectoral fin insertions, not forming a shallow groove.

Rostral cartilage broad, its shaft increasing slightly in width posteriorly; rostral node rounded at apex, not angular, relatively short, axis at widest point of node 29.17% (36.7–40.5%) of length of rostral cartilage from snout tip; precerebral fontanelle broad and convex; rostral cartilage 73.9% (68.7–71.6%) of length of neurocranium; nasal capsules rather large, their transverse axes anterolaterally directed; maximum width across capsules 1.06 (1.03–1.08) times nasobasal length of cranium (base of rostrum to occipital condyles); nasal capsule length slightly greater than width; basal plate minimum width 2.73 (2.78–3.16) times in nasobasal length; anterior cartilage triangular, posterior wedge-shaped.

Pectoral skeleton with 32–33 (32) preopterygial, 8 (8) mesopterygial, 2 (1–2) neopterygial, 29 (24–29) metapterygial, amounting to 71–72 (66–70) total radials. Total pelvic radials 28–29 (26–28). Total vertebral segment (synarcual and free) counts 209 (199–201), post-synarcural centra 194 (185–186), precaudal centra (excluding synarcural centra) 156 (147–149); synarcural segments 15 (14–15); monospondylous precaudal centra 52 (39); diplospondylous precaudal centra 104 (108–110), diplospondylous caudal centra 38 (37–38). Monospondylous to diplospondylous centra transition posterior to pelvic fin girdle.

Distribution. The distribution of *R. holcorhynchus* broadly overlaps with *R. austini* from Port Shepstone, southern KwaZulu-Natal Province, South Africa to north of Bazaruto Island, central Mozambique. Although they overlap geographically, *R. holcorhynchus* appears to occur more offshore and in deeper waters (75–254 vs. <1–107 m) than *R. austini* (Wallace 1967, Ebert & Gon 2017).

Remarks. Prior to this project, the most comprehensive descriptions of *R. holcorhynchus* were the redescriptions by Norman (1926) and Wallace (1967), which are both lacking by modern standards. The redescription by Norman (1926) expanded his original species description from 1922, which did not quantify the morphological characters described by percent total length and did not include most of the morphological measurements used today. However, his redescription still lacked the majority of measurements used today and several morphometrics were measured in a different way (see Weigmann 2011 for comments). The subsequent redescription of *R. holcorhynchus* by Wallace (1967) was the most comprehensive species account to date but still contained only 31 morphological measurements, less than half the measurements used today. Many of the missing measurements include characters related to body size (e.g. head length and snout to lower caudal fin origin), fin morphology (e.g. dorsal fin inner margin lengths), and the nasal region (e.g. anterior, posterior, and posterolateral nasal flap morphologies). No detailed redescription of *R. holcorhynchus* has been published since Wallace (1967), more than 55 yr ago. There are several differences in the proportional body width and depth measurements between the subadult holotype and juvenile individuals; however, these are likely due to the eviscerated status of the holotype.

R. holcorhynchus is morphologically most similar to *R. austini*. Although the proportional size of many morphometric characters overlaps between the 2 species, *R. holcorhynchus* can be distinguished by proportionally longer ventral head length (27.7–28.2 vs. 25.9–27.4% TL), presocket snout length (15.2–16.0 vs. 12.7–15.1% TL), and distance across anterior nasal apertures (9.3–10.5 vs. 6.7–9.2% TL). *R. holcorhynchus* also has a proportionally narrower body depth at the second dorsal fin origin (2.3–2.4 vs. 2.6–3.2% TL). The anterior nasal flap of *R. holcorhynchus* extends to the inner edge of the nostril but not into internarial space, while the anterior nasal flap of *R. austini* extends into internarial space. *R. holcorhynchus* also has more nasal lamellae than *R. austini* (68–75 vs. 61–64). All *R. holcorhynchus* individuals (juveniles and adult) and male *R. austini* possess thorns along the midback; however, the thorns of the adult *R. holcorhynchus* along the midback are much more pronounced than those of *R. austini*. The adult male *R. holcorhynchus* also possesses scapular thorns (3 vs. 0) and has more thorns between the dorsal fins (6 pronounced thorns and 3–4 minute thorns vs. 1–3 pronounced thorns) than *R. austini*.

In terms of coloration, *R. holcorhynchus* and *R. austini* both possess a teardrop-shaped dark blotch on the ventral surface of the snout, which has contributed to the misidentification of these 2 species. Both species also have a somewhat translucent rostrum flanking the rostral cartilage. The dorsal surface of *R. holcorhynchus*, however, is dark olive green with no spots, markings, or patterns, while *R. austini* has a color pattern of paired spots, occasionally forming dark transverse bands. After preservation, the dorsal surface of *R. holcorhynchus* turns brownish while the ventral surface darkens to a brownish grey. The outer margins of pectoral and

pelvic fins also become slightly lighter on both dorsal and ventral surfaces.

R. holcorhynchus appears to exhibit several differences in body proportions between the juvenile female and males (juveniles and adult) that may indicate sexual dimorphism. The juvenile female had a proportionally longer preoral length (18.2 vs. 18.0% TL), shorter pelvic fin inner margin length (5.6 vs. 6.4–7.2% TL), and longer posterior nasal flap base length (3.5 vs. 2.6–3.0% TL). However, sexually mature adult *R. holcorhynchus* specimens, especially females, are needed to establish the extent of sexual dimorphism in adults. Additional juvenile and adult specimens from both sexes are also needed to clarify ontogenetic change within this species. Furthermore, the tooth row counts of the juvenile specimens, i.e. 41–47, indicated by Wallace (1967) are much lower than our counts of the subadult male holotype. Although ontogenetic changes in tooth row counts are conceivable, the counts by Wallace (1967) may be incorrect as erroneous counts in Wallace (1967) were detected by Weigmann (2011) for another guitarfish, *Rhynchobatus djiddensis*. The erroneous values are probably based on counting only the parallel transverse rows instead of the pavement pattern (Weigmann 2011).

3.2.3. *Rhinobatos nudidorsalis* Last, Compagno & Nakaya, 2004

Bareback guitarfish or bareback shovelnose ray (Figs. 5–7, 13 & 14; Tables 1–3, Table S7)

Material examined. Four specimens. (1) Holotype, HUMZ 81478, mature male 501 mm TL, Mascarene Ridge, 10° 46′ S, 60° 05′ E, 125 m depth, 10 December 1978; (2) SAIAB 84016, mature male 673 mm TL, 214–219 m depth, Mascarene Ridge, 16° 27.62′ S, 60° 16.84′ E, RV 'Dr Fridtjof Nansen' trawl, 14 October 2008; (3) SAIAB 84037, mature male 695 mm TL, 214–219 m depth, Mascarene Ridge, 16° 27.62′ S, 60° 16.84′ E RV 'Dr Fridtjof Nansen' trawl, 14 October 2008; (4) ZMH 25548, gravid female 753 mm TL (fresh), 740 mm TL (preserved), Saya de Malha Bank, 11° 21.6′ S, 61° 46.8′ E–11° 22.2′ S, 61° 44.5′ E, 87–110 m depth, RV 'Vityaz' cruise 17, Stn 2803, 29 m shrimp trawl, Trawl #83, 7 January 1989.

Diagnosis. A small species of *Rhinobatos* (attaining at least 753 mm TL) distinguished by the following combination of characters: snout bluntly pointed, length 4.6–5.2 times interorbital width; ventral head length 25.5–27.3% TL; presocket snout length 14.6–15.2% TL; nostrils diagonal, their length 1.6–1.8 times internarial distance; mouth width 5.0–5.3% TL; ante-

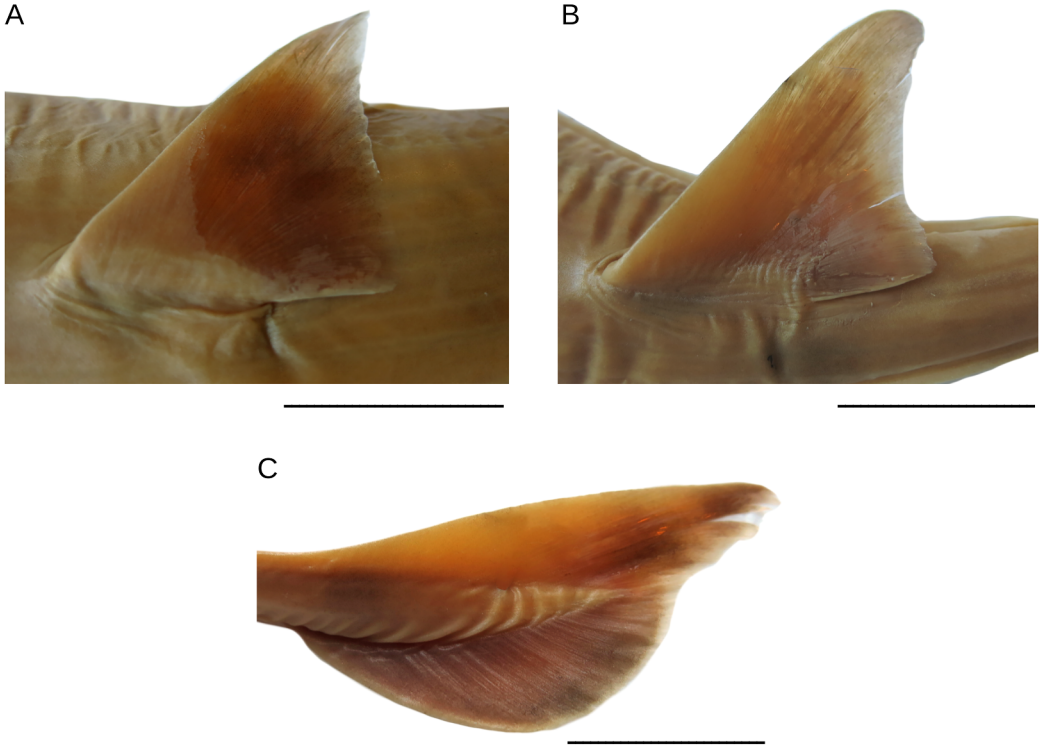

Fig. 13. *Rhinobatos nudidorsalis*, male, 673 mm total length (TL) (SAIAB 84016), preserved. Lateral views of (A) the first dorsal fin, scale bar = 3 cm; (B) the second dorsal fin, scale bar = 3 cm; (C) the caudal fin, scale bar = 2 cm. Photographs courtesy © Marsha Englebrecht

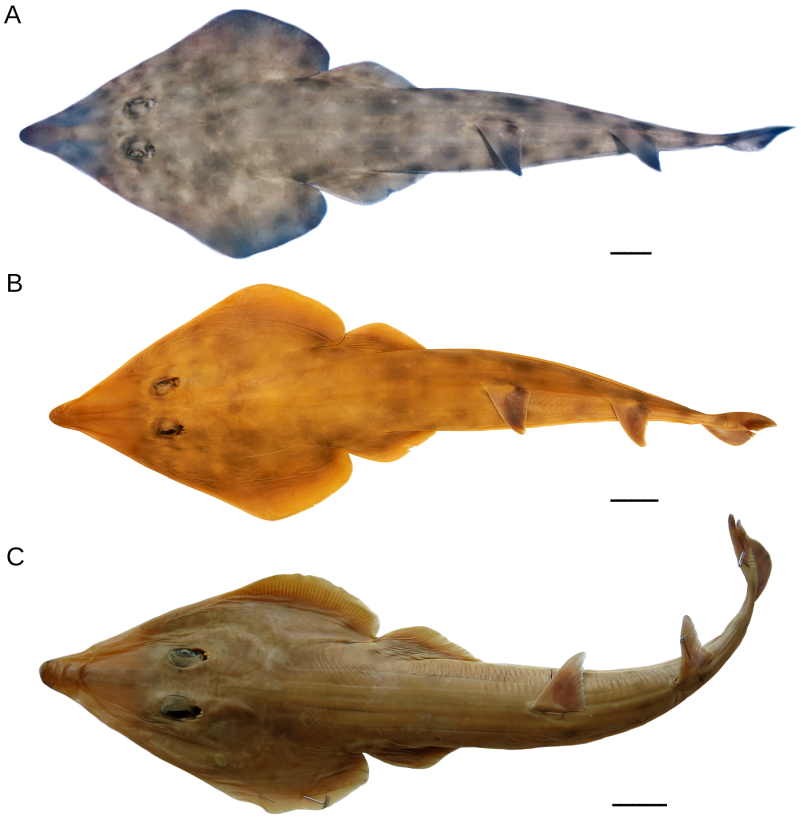

Fig. 14. Variations in spot pattern of *Rhinobatos nudidorsalis* with preservation. (A) Female, 753 mm total length (TL) (ZMH 25548), fresh. Spot pattern apparent. (B) Female, 740 mm TL (ZMH 25548), preserved. Spot pattern faded. (C) Male, 673 mm TL (SAIAB 84016), preserved. Spot pattern mostly obscure. Scale bars = 5 cm. Photographs courtesy (A) © Matthias Stehmann, (B) © Simon Weigmann, (C) © Marsha Englebrecht

rior nasal flaps inserted into internarial space; posterior nasal flaps lobe-like, inner edges not reaching the innermost margin of the nostril; spiracles fairly small and narrowly bean-shaped; gill openings sinusoidal; distance between fifth gill slits 3.1–3.7 times internarial distance; post-scapular sensory canals long, terminating just anterior to pectoral fin insertions; dermal denticles close-set, mostly minute, not covering entire body and fins, thorns and tubercles absent; dorsal fins relatively tall, height of first 7.0–7.9% TL; body depth at second dorsal fin origin 5.0–5.3% TL; tooth row counts in lower and upper jaws 78–79; 45–55 nasal lamellae; 189–201 total (synarcual and free) vertebral segments, 34–36 monospondylous precaudal centra, all with ribs, 30–40 diplosondylous caudal centra, monospondylous to diplosondylous centra transition posterior to pelvic fin girdle; dorsal surface light to medium yellowish brown, rostral cartilage slightly translucent, may have a variable spot pattern when fresh that fades considerably after preservation; ventral surface mostly plain except for black line along each side of ventral snout and males with a singular medium to dark brown spot nearly in line with exterior edge of aperture, anterior to mouth on both sides; no teardrop shaped blotch on underside of snout.

Distribution. *R. nudidorsalis* is the only species of *Rhinobatos* currently known from the Mascarene Ridge where it may possibly be endemic. All other WIO *Rhinobatos* species occur either along the east coast of Africa and along Madagascar (*R. austini* and *R. holcorhynchus*) or in the northern Indian Ocean (*R. annandalei*, *R. lionotus*, and *R. punctifer*).

Remarks. The original description of *R. nudidorsalis* was based on the holotype (HUMZ 81478), the only known specimen, which was collected from the Mascarene Ridge (Last et al. 2004). For the purposes of this study, a new radiograph of the holotype was taken. The total number of vertebrae, monospondylous centra, and diplospondylous caudal centra reported in Last et al. (2004) were 180, 23, and 31, respectively. From the new radiograph, the total number of vertebrae, monospondylous centra, and diplospondylous caudal centra were 189, 26, and 40, respectively.

The new specimens described here are all much larger than the holotype (501 vs. 673–753 mm TL).

There was a notable difference in the number of nasal lamellae between the holotype and new material (45 vs. 50–55). Other notable differences between the holotype and the new material examined here include differences in nasal lamellae, and vertebral counts. The holotype had 45 nasal lamellae, while the 3 new specimens had nasal lamellae counts of 50–55. Similarly, the total number of vertebrae, monospondylous centra and diplospondylous precaudal centra were 189, 26, and 109, respectively. From the radiographs of 2 males and female, the total number of vertebrae and monospondylous centra were much higher, 199–201 and 34–36, respectively. The 2 males also had higher diplospondylous precaudal centra counts, 119–120. The radiograph of the female, however, showed the same number of diplospondylous precaudal centra as the holotype (109). The proportional values of each morphological character for the new material were similar to the holotype.

R. nudidorsalis is morphologically similar to *R. holcorhynchus* and was previously often misidentified as *R. holcorhynchus,* including in museum collections. While there is an overlap in several morphometric characters, *R. nudidorsalis* can be distinguished by a proportionally shorter dorsal head length (19.9–27.2 vs. 28.5–30.7% TL), ventral head length (25.5–27.3 vs. 27.7–28.2% TL), snout to pelvic-fin origin (37.2–38.6 vs. 39.0.–39.8% TL), orbit and spiracle length (4.2–5.2 vs. 5.6–6.9% TL), interorbital width (2.9–3.3 vs. 3.5–4.3% TL), mouth width (5.0–5.3 vs. 6.1–7.2% TL), and distance between fifth gill openings (7.5–8.0 vs. 8.7–12.8% TL). In addition, the anterior nasal flaps of *R. nudidorsalis* extend into internarial space while the anterior nasal flaps of *R. holcorhynchus* extend to the inner edge of the nostril but not into internarial space. In terms of meristics, *R. nudidorsalis* possesses no thorns on the dorsal surface while *R. holcorhynchus* has prominent thorns along the midback and between the dorsal fins, as well as scapular thorns. Similarly, male *R. austini* have thorns along the midback and between the dorsal fins. *R. Nudidorsalis* also has fewer nasal lamellae than *R. holcorhynchus* (45–55 vs. 68–75).

Since the original description of *R. nudidorsalis* was based on a single male individual, this rediagnosis provides the first range of sizes for this species in addition to the first female. *R. nudidorsalis* appears to exhibit several differences in morphology between the female and males. The female has a longer disc (41.5 vs. 39.1–41.2% TL), shorter ventral head length (25.5 vs. 26.0–27.3% TL), and greater disc width at anterior orbit (18.1 vs. 15.5–16.9% TL). There are also differences in many of the proportional body width and depth measurements; however, these are likely due to the gravid status of the female measured. Therefore, additional specimens, especially non-gravid females, are needed to establish the extent of this variability within males and females and between males and females.

After preservation, the dorsal surface of *R. nudidorsalis* becomes light to medium yellowish brown and the rostral cartilage slightly translucent. After 30 yr, spots are faded but still visible on the preserved female. On the males, however, the spots are difficult to see after only 10 yr of preservation, and the male holotype showed no spots after 25 yr of preservation. For both sexes, the ventral surface darkens slightly after preservation and the black lines along each side of ventral snout becomes slightly faded. The singular medium to dark brown spot nearly in line with exterior edge of aperture on both sides of the mouth in males also fades slightly.

Although most *Rhinobatos* species show consistent coloration within species, other species of *Rhinobatos* demonstrate considerable color variations between individuals. *R. punctifer* has 3 different color morphs — a white-spotted morph, a plain morph, and an ocellated morph (Last et al. 2019). Similarly, young *R. schlegelii* possess a teardrop-shaped blotch on the ventral surface of the snout (similar to *R. austini* and *R. holcorhynchus*) that typically becomes obscure in adults (Ebert & Gon 2017). In other *Rhinobatos*, preservation may also impact coloration where fresh specimens have a distinguishable spot pattern and preserved specimens do not. For example, the spots on *R. borneensis* Last, Séret & Naylor, 2016 are apparent when fresh but become obscure or appear as pale blotches after preservation (Last et al. 2016). Therefore, fresh males and more females are needed to describe this variation in detail.

4. DISCUSSION

Guitarfish species are morphologically very similar and, as a result, they are often difficult to distinguish. Combined with vague original descriptions, these morphological similarities can lead to misidentifications that can leave species vulnerable to mismanagement and exploitation. The SWIO *Rhinobatos* are a clear example of this, where the brief original description of *R. holcorhynchus* has led to the confusion with *R. austini* and *R. nudidorsalis*, making it difficult for these species to be assessed other than Data Deficient.

Although these 3 species are very similar in appearance, the present study shows they are morpho-

logically distinct based on differences in their morphometrics, meristics, and color pattern. Multivariate statistics were run to evaluate the morphological differences between WIO *Rhinobatos* species and confirm the validity of the 3 SWIO species. Although the results of the analyses varied slightly, the 3 SWIO species formed clusters and showed separation that was on par with the 4 other Indian Ocean *Rhinobatos* species. This further clarifies that *R. austini*, *R. holcorhynchus*, and *R. nudidorsalis* are distinct species.

Several characters that loaded into the PCA and LDAs matched which characters from the traditional morphological analysis were distinct between species. For the PCA, presocket snout length and mouth width primarily loaded into either PC1 or PC2. *R. austini* had a shorter presocket snout length (12.7–15.1 vs. 15.2–16.0% TL) than *R. holcorhynchus* while *R. nudidorsalis* had a narrower mouth than both *R. austini* and *R. holcorhynchus* (5.0–5.3 vs. 5.4–6.2 and 6.0–7.2% TL, respectively). For the LDAs, distance across anterior nasal apertures primarily loaded into LD1 and LD2 at least once. *R. holcorhynchus* had a larger distance across anterior nasal apertures than *R. austini* and *R. nudidorsalis* (9.3–10.5 vs. 6.7–9.2 and 8.4–9.3% TL, respectively). Some of these characters are also morphologically distinct for other Indian Ocean *Rhinobatos*. For example, *R. ranongensis* had a longer snout length than *R. punctifer* and a shorter snout length than *R. jimbarensis* Last, White & Fahmi, 2006. Similarly, *R. annandalei* had a wider mouth width than *R. lionotus* and *R. punctifer* (Last et al. 2019).

Some characters that are useful for distinguishing other species of *Rhinobatos* based on traditional morphological analysis were not as informative for the 3 SWIO *Rhinobatos*. For example, disc width maximum can be used to distinguish *R. borneensis* from *R. whitei* Last, Corrigan & Naylor, 2014, as well as *R. annandalei* from *R. lionotus* and *R. punctifer* (Last et al. 2016, 2019). For the SWIO *Rhinobatos*, however, there were no noticeable differences between the maximum disc width for all 3 species. Disc width maximum also never primarily loaded into the PCA or LDAs. Nasal morphology, however, appeared to be very informative in distinguishing these species.

The LDA performed on the nasal region for the 3 SWIO species showed more separation than the LDAs performed on nasal characters of the 7 Indian Ocean species and the Gulf of California *Pseudobatos* (Rutledge 2019). This LDA also showed more separation and clustering than the LDA performed on all 63 measurements for the SWIO *Rhinobatos*. The primary linear discriminant loadings for the LDAs performed on nasal morphology were similar to those reported in Rutledge (2019), such as anterior nasal flap base length, nostril length, and distance from nostril to disc margin.

The demonstrated effectiveness of nasal morphology in distinguishing species of *Rhinobatos*, especially those from the SWIO, emphasizes the importance of measuring these characters with precision. This also indicates that the nasal region alone may be more useful in distinguishing SWIO *Rhinobatos* species than using all 63 morphological characters, supporting the notion that some characters are ineffective as taxon identifiers within genera (Last et al. 2019, Rutledge 2019).

Some of the more prominent differences between species were not reflected in the morphometric measurements evaluated by the statistical analyses (e.g. dorsal surface coloration, presence and number of dorsal thorns and tubercles, and meristics). There was no overlap between the number of nasal lamellae for each of these 3 species, indicating that this is a reliable method for distinguishing them. These differences in nasal lamellae counts are greater than those reported for other Indian Ocean *Rhinobatos* species, where the nasal lamellae counts for *R. annandalei* and *R. punctifer*, and *R. lionotus* and *R. ranongensis* have some overlap (Last et al. 2019). This is particularly noteworthy since counting nasal lamellae does not require specialized training. Nasal lamellae counts also do not require the individual to be intact, which may be useful for identifying individuals in the field or at fish markets.

The dorsal surface also varies greatly between each species. For coloration especially, *R. austini* possesses a banding pattern of spots, but *R. holcorhynchus* does not have any spots or patterning. *R. holcorhynchus* is also considerably darker than *R. nudidorsalis*. In addition, *R. nudidorsalis* possesses no thorns or tubercles on the dorsal surface, which contrasts sharply with the thorns that run along the midback of *R. holcorhynchus*. Although both male *R. austini* and *R. holcorhynchus* possess thorns along the midback, *R. holcorhynchus* has considerably more thorns between the dorsal fins (6–18 vs. 1–3) and the second dorsal fin and caudal fin (3–9 vs. none) than *R. austini*. Similarly, female *R. holcorhynchus* possess thorns while female *R. austini* have none.

The rediagnoses of *R. austini*, *R. holcorhynchus*, and *R. nudidorsalis* presented here highlight the subtle, yet distinguishing characteristics of these species by incorporating new material. This study is the first time a male and a female have been described for *R. austini* and *R. nudidorsalis*, respectively, enhancing our understanding of the morphology and sexual

dimorphism of these species. Similarly, the redescription of *R. holcorhynchus* presented here includes the first description of the chondrocranium. These rediagnoses are also critical to improving the identification of these species relative to each other and clarifying their statuses. In addition to providing the taxonomic foundation for future life history studies to determine basic life history characteristics, these rediagnoses should allow for more confident identifications for future molecular studies. The redefinitions of these 3 species should also be used as a basis for updating their IUCN Red List Assessments (Pollom et al. 2019, Pollom & Ebert 2019a,b).

In November 2022, the Convention for International Trade in Endangered Species (CITES) listed all members of Rhinobatidae under Appendix II (CITES 2022). This listing indicates that they are not necessarily threatened with extinction but may become so unless trade is regulated. Since most guitarfishes (Rhinobatidae) are assessed as Vulnerable or higher by the IUCN, improved fisheries monitoring and the development of additional management plans are necessary to further mitigate this extinction risk. A coordinated effort is still required to collect more material across a range of sexes and sizes to capture ontogenetic variability, which has been described for few *Rhinobatos* species (Last et al. 2019). More material is also needed to further clarify the geographic range of each species (Fig. 15). The other WIO *Rhinobatos* species do not geographically overlap with the 3 SWIO *Rhinobatos*; however, the extent of the geographic overlap between *R. austini* and *R. holcorhynchus* remains unclear. *R. nudidorsalis* appears to have the most restricted range of the 3 SWIO species; however, further surveys of the surrounding area are needed to determine whether this species is indeed endemic to the Mascarene Ridge (Last et al. 2004).

In the first global assessment of Chondrichthyan species in 2014, 24% were threatened with extinction (Dulvy et al. 2014). In less than a decade, that number has grown to 32.6% (Dulvy et al. 2021a). A number of species that were previously Data Deficient were reassessed by the IUCN between both global assessments, including one WIO guitarfish, *R. annandalei*. *R. annandalei* was redescribed in 2019 and subsequently reassessed as Critically Endangered (Dulvy et al. 2021a, Johri et al. 2021). A similar situation may become apparent for the SWIO *Rhinobatos*, emphasizing the urgent need to further study the biology (age and growth, age at maturity, and diet) and distribution (depth and geographic ranges) of these species so they can be reassessed by the IUCN.

5. ADDITIONAL MATERIAL EXAMINED

5.1. *Rhinobatos annandalei* Norman, 1926

Seven specimens: (1) lectotype, BMNH 1909.7.12.1, 423 mm TL, immature male, Bay of Bengal, east channel, mouth of Hooghly River, India, ~70 m depth; (2) paralectotype, BMNH 1909.7.12.2, 398 mm TL, female, Bay of Bengal, east channel, mouth of Hooghly River, India, ~70 m depth (collected with BMNH 1909.7.12.1); (3) SAIAB 208954, 253 mm TL, female, RV 'Dr Fridtjof Nansen' Sri Lanka Survey, 2018; (4) CSIRO H 7866-01, 870 mm TL, female Bay of Bengal, N of Andaman Is, Myanmar, 14° 40.56' N, 93° 44.93' E, bottom trawl, 88 m depth, RV 'Dr Fridtjof Nansen' Stn 59, collected P. Psomadakis, 9 May 2015; (5) CSIRO H unregistered #25, 621 mm TL, female, probably Karachi fish market, Pakistan, 12 Oct 2013; (6) PMBC 6736, 493 mm TL, female, northern Andaman Sea, Myanmar, 90–140 m depth, 3 Nov 1989; (7) unregistered 881 mm TL, male, Stn 113, RV *Dr Fridtjof Nansen* Myanmar Survey, 2018.

5.2. *Rhinobatos lionotus* Norman, 1926

Eleven specimens: (1) holotype, BMNH 1909.7.12.3, female 495 mm TL, mouth of Hooghly River, India, ~70 m depth; (2) CSIRO H 7867-01, female 760 mm TL, Bay of Bengal, N of Andaman Is, Myanmar, 15° 01.63' N, 93° 45.55' E, bottom trawl, 76 m depth, RV 'Dr Fridtjof Nansen' Stn 60, specimen 247, collected P. Psomadakis, 9 May 2015; (3) Stn 41, female 640 mm TL, Nansen Myanmar survey, 2018; (4) SAIAB 209323, female 630 mm TL, Sri Lanka Survey, Stn 6, 2018; (5) SAIAB 209325, female 825 mm TL, Nansen Myanmar survey, Stn 119, 2018; (6) Stn 104, female 506 mm TL, Nansen Myanmar survey, 2018; (7) Stn 104, male 440 mm TL, Nansen Myanmar survey, 2018; (8) Stn 104, male 395 mm TL, Nansen Myanmar survey, 2018; (9) SAIAB 209326, female 430 mm TL, Nansen Myanmar survey, Stn 119, 2018; (10) SAIAB 209324, male 444 mm TL, Nansen Myanmar survey, Stn 119, 2019; (11) SAIAB 209321, female 632 mm TL, Sri Lanka survey, Stn 5, 2018.

5.3. *Rhinobatos punctifer* Compagno & Randall, 1987

Two specimens: (1) holotype, BPBM 20843, male 705 mm TL, Red Sea, Gulf of Aqaba, Israel; (2) unregistered, male 619 mm TL, Pakistan.

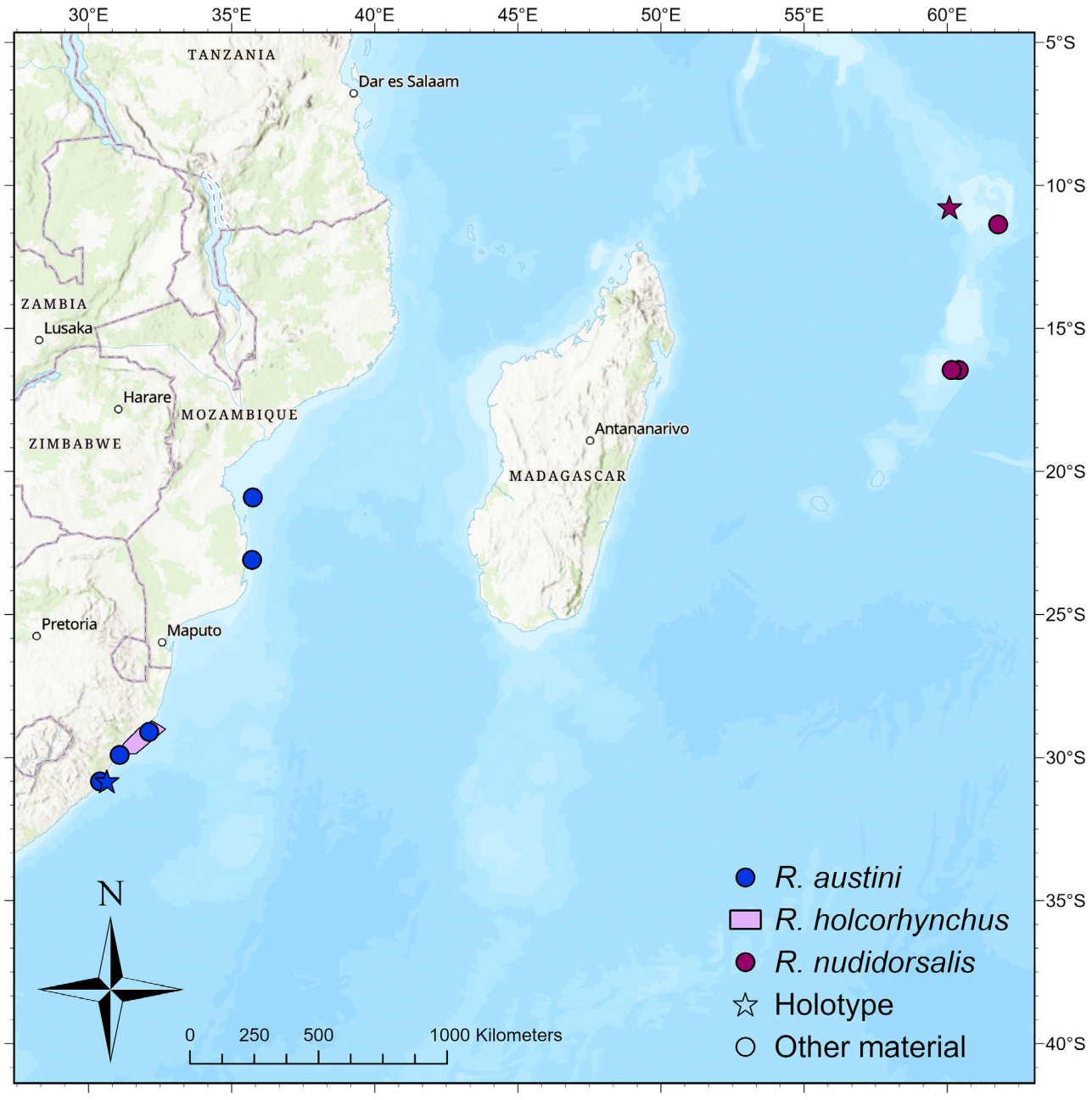

Fig. 15. The distributions of *Rhinobatos austini* (blue), *R. holcorhynchus* (pink), and *R. nudidorsalis* (magenta) based on material examined. Stars: type locality of the holotypes; circles: localities of other material. A range is given for *R. holcorhynchus* based on approximate locations of material examined

5.4. *Rhinobatos ranongensis* Last, Séret & Naylor, 2019

Four specimens: (1) holotype, CSIRO H 7861-02, male 645 mm TL, Andaman Sea, W of Maliwun, Myanmar, 10° 20.97′ N, 97° 46.14′ E, bottom trawl, 69 m depth, RV 'Dr Fridtjof Nansen', Stn 173, collected P. Psomadakis, 25 May 2015; (2) paratype, CSIRO H 8403-01 (formerly SA005), male 494 mm TL, Ranong fish landing, collected S. Arunrugstichai, 17 July 2014; (3) paratype, CSIRO H 8404-01 (formerly SA043), male 425 mm TL; (4) paratype, CSIRO H 8404-02 (formerly SA045), female 392 mm TL, Ranong fish landing, collected S. Arunrugstichai, 22 January 2015.

Acknowledgements. The present work was part of R.M.A.'s Master's thesis. For their assistance with data collection, the authors thank Peter Last (CSIRO) for providing data for the 4 Indian Ocean species, Dave Catania and Jon Fong (CAS) for providing collection support and radiographs, Kyle Luckenbill and Mark Sabaj (ANSP) for providing

radiographs of the *Rhinobatos natalensis* holotype, John Pogonoski (CSIRO) for providing radiographs of the *R. nudidorsalis* holotype, Irina Eidus and Thilo Weddehage (ZMH) for providing radiographs of the ZMH *R. nudidorsalis* specimen, and James Maclaine, Chrissy Williams, Harry Taylor, and Lucie Goodayle (BMNH) for providing photographs and a radiograph of the *R. holcorhynchus* holotype. General assistance, photographs, and support were kindly provided by Bruce Mann, Ryan Daly, and Sean Fennessy (Oceanographic Research Institute), Rhett Bennett (Wildlife Conservation Society), Michaela van Staden and Aletta Bester-van der Merwe (University of Stellenbosch), Angus Paterson, Roger Bills, Nkosinathi Mazungula, Paul Cowley, Mzwandie Dwani, Vuyani Hanisi, Elaine Heemstra, and Ofer Gon (SAIAB), Marsha Englebrecht, and Shawn Melendy. S.W. is also grateful to Ralf Thiel (ZMH) for granting access to specimens in the ZMH collection and access to radiography facilities at ZMH, Irina Eidus (ZMH) for her help with the radiography and collection database, and Matthias F. W. Stehmann (ICHTHYS), who collected the ZMH specimen of *R. nudidorsalis* and kindly provided the fresh photograph and granted permission for use in the present paper. Funding support for this project was provided by the Save Our Seas Foundation Keystone Grant 431, South African Shark and Ray Protection Project, implemented by the WILDTRUST, funded by the Shark Conservation Fund, Andrew Sabin Family Foundation, California State University Monterey Bay, Moss Landing Marine Laboratories, and San Jose State University and the South African Institute for Aquatic Biodiversity. Open Access funding was provided by the Save Our Seas Foundation. This paper was presented at the Global Symposium on wedgefish and guitarfish, a symposium of the American Elasmobranch Society, with funding support from the Save Our Seas Foundation. This paper was also presented at the 2022 American Elasmobranch Society meeting in Spokane, WA, USA. The authors thank the Save Our Seas Foundation for generous financial assistance towards publication of this manuscript and for their support of the American Elasmobranch Society Global Wedgefish & Guitarfish Symposium 2021. The Symposium was further supported by the Pacific Shark Research Center (Moss Landing Marine Laboratories), Dallas World Aquarium, Charles Darwin University, and the Georgia Aquarium.

LITERATURE CITED

Barnard KH (1925) A monograph of the marine fishes of South Africa. Part I (Amphioxus, Cyclostomata, Elasmobranchii, and Teleostei-Isospondyli to Heterosomata). Ann S Afr Mus 21:1–418

Barnard KH (1927) A monograph of the marine fishes of South Africa. Part II (Teleostei– Discocephali to end. Appendix). Ann S Afr Mus 21:419–1065

Barnard KH (1959) A pictorial guide to South African fishes, marine and freshwater. Maskew Miller, Cape Town

CITES (2022) Summary record of the fourth plenary session In: Summary records. CoP19 Plen. Rec. 4. CITES, Geneva, p 2

Compagno LJV (1986) Families Pristidae, Narkidae, Rhinobatidae, Myliobatidae, Mobulidae, Dasyatidae, Chimaeridae, Rhinochimaeridae, Callorhinchidae. In: Smith MM, Heemstra, PC (eds) Smith's sea fishes. Macmillan, Johannesburg, p 110–142, 144–147

Compagno LJV (1999) An overview of chondrichthyan systematics and biodiversity in southern Africa. Trans R Soc S Afr 54:75–120

Compagno LJV, Ebert DA, Smale MJ (1989) Guide to the sharks and rays of Southern Africa. New Holland, London

da Silva C, Booth AJ, Dudley SFJ, Kerwath SE and others (2015) The current status and management of South Africa's chondrichthyan fisheries. Afr J Mar Sci 37: 233–248

Dulvy NK, Fowler SL, Musick JA, Cavanagh RD and others (2014) Extinction risk and conservation of the world's sharks and rays. eLife 3:e00590

Dulvy NK, Pacoureau N, Rigby CL, Pollom RA and others (2021a) Overfishing drives over one- third of all sharks and rays toward a global extinction crisis. Curr Biol 31: 4773–4787.e8

Dulvy NK, Akhilesh KV, Bineesh KK, Derrick D and others (2021b) *Rhinobatos annandalei*. The IUCN Red List of Threatened Species 2021: T161478A124492224. https://dx.doi.org/10.2305/IUCN.UK.2021-2.RLTS.T161478A124492224.en

Dulvy NK, Bineesh KK, Derrick D, Fernando D, Haque AB, Maung A, VanderWright WJ (2021c) *Rhinobatos lionotus*. The IUCN Red List of Threatened Species 2021: T161677A124526883. https://dx.doi.org/10.2305/IUCN.UK.2021-2.RLTS.T161677A124526883.en

Dulvy NK, Bineesh KK, Derrick D, Fernando D, Haque AB, Maung A, Sherman CS (2021d) *Rhinobatos ranongensis*. The IUCN Red List of Threatened Species 2021: T176486239A176486247. https://dx.doi.org/10.2305/IUCN.UK.2021-2.RLTS.T176486239A176486247.en

Ebert DA (2013) Deep-sea cartilaginous fishes of the Indian Ocean, Vol 1. Sharks. In: Mostarda E (ed) FAO species catalogue for fishery purposes, Vol 1. FAO, Rome

Ebert DA, Gon G (2017) *Rhinobatos austini* n. sp., a new species of guitarfish (Rhinopristiformes: Rhinobatidae) from the Southwestern Indian Ocean. Zootaxa 4276: 204–214

Ebert DA, van Hees KE (2015) Beyond jaws: rediscovering the 'lost sharks' of southern Africa. Afr J Mar Sci 37:141–156

Ebert DA, Khan M, Ali M, Akhilesh KV, Jabado RW (2017) *Rhinobatos punctifer*. The IUCN Red List of Threatened Species 2017: T161447A109904426. https://dx.doi.org/10.2305/IUCN.UK.2017-2.RLTS.T161447A109904426.en

Ebert DA, Wintner SP, Kyne PM (2021) An annotated checklist of the chondrichthyans of South Africa. Zootaxa 4947: 001–127

Ferrando S, Gallus L, Ghigliotti L, Amaroli A, Abbas G, Vacchi M (2017) Clarification of the terminology of the olfactory lamellae in Chondrichthyes. Anat Rec (Hoboken) 300:2039–2045

Fowler HW (1925) Fishes from Natal, Zululand and Portuguese East Africa. Proc Acad Nat Sci Philadelphia 77: 187–268

Fowler HW (1941) The fishes of the groups Elasmobranchii, Holocephali, Isospondyli, and Ostarophysi obtained by the U.S. Bureau of Fisheries streamer 'Albatross' in 1907 to 1910, chiefly in the Philippine Islands and adjacent seas. Bull US Natl Mus 100:1–879

Fricke R, Mahafina J, Behivoke F, Jaonalison H, Léopold M, Ponton D (2018) Annotated checklist of the fishes of Madagascar, southwestern Indian Ocean, with 158 new records. FishTaxa 3:1–432

Heemstra PC, Heemstra E (2004) Coastal fishes of Southern Africa. National Inquiry Service Centre and South African

Institute for Aquatic Biodiversity, Grahamstown
Jabado RW (2018) The fate of the most threatened order of elasmobranchs: shark-like batoids (Rhinopristiformes) in the Arabian Sea and adjacent waters. Fish Res 204: 448–457
Jabado RW, Kyne PM, Pollom RA, Ebert DA, Simpfendorfer CA, Ralph GM, Dulvy NK (2017) The conservation status of sharks, rays, and chimaeras in the Arabian Sea and adjacent waters. Environment agency — Abu Dhabi, UAE, and IUCN Species Survival Commission Shark Specialist Group, Vancouver
Johri S, Fellows SR, Solanki J, Busch A and others (2020) Mitochondrial genome to aid species delimitation and effective conservation of the sharpnose guitarfish (*Glaucostegus granulatus*). Meta Gene 24:100648
Johri S, Livingston I, Tiwari A, Solanki J and others (2021) Reducing data deficiencies: preliminary elasmobranch fisheries surveys in India, identify range extensions and large proportions of female and juvenile landings. Front Mar Sci 8:619695
Kyne PM, Jabado RW, Rigby CL, Dharmadi and others (2020) The thin edge of the wedge: extremely high extinction risk in wedgefishes and giant guitarfishes. Aquat Conserv 30:1337–1361
Last PR, White WT, Fahmi (2006) *Rhinobatos jimbaranensis* and *R. penggali*, two new shovelnose rays (Batoidea: Rhinobatidae) from eastern Indonesia. Cybium 30:261–271
Last PR, Compagno LJV, Nakaya K (2004) *Rhinobatos nudidorsalis*, a new species of shovelnose ray (Batoidea: Rhinobatidae) from the Mascarene Ridge, Central Indian Ocean. Ichthyol Res 51:153–158
Last PR, Corrigan S, Naylor G (2014) *Rhinobatos whitei*, a new shovelnose ray (Batoidea: Rhinobatidae) from the Philippine Archipelago. Zootaxa 3872:31–47
Last PR, Séret B, Naylor GJP (2016) A new species of guitarfish, *Rhinobatos borneensis* sp. nov. with a redefinition of the family-level classification in the order Rhinopristiformes (Chondrichthyes: Batoidea). Zootaxa 4117:451–475
Last PR, Séret B, Naylor GJP (2019) Description of *Rhinobatos ranongensis* sp. nov. (Rhinopristiformes: Rhinobatidae) from the Andaman Sea and Bay of Bengal with a review of its northern Indian Ocean congeners. Zootaxa 4576:257–287
Moore ABM (2017) Are guitarfishes the next sawfishes? Extinction risk and an urgent call for conservation action. Endang Species Res 34:75–88
Norman JR (1922) Three fishes from Zululand and Natal, collected by Mr H.W. Bell Marlet; with additions to the fish fauna of Natal. Ann Mag Nat Hist 9:318–322
Norman JR (1926) A synopsis of the rays of the family Rhinobatidae, with a revision of the genus *Rhinobatus.* Proc Zool Soc Lond 96:941–982
NPOA (2013) National plan of action for the conservation and management of sharks (NPOA – sharks). Department of Agriculture, Forestry and Fisheries (DAFF), Rogge Bay, Cape Town
Pollom R, Ebert DA (2019a) *Rhinobatos austini.* The IUCN Red List of Threatened Species 2019: T124396530A124552542. https://dx.doi.org/10.2305/IUCN.UK.2019-3.RLTS.T124396530A124552542.en
Pollom R, Ebert DA (2019b) *Rhinobatos nudidorsalis.* The IUCN Red List of Threatened Species 2019: T60169A124447127. https://dx.doi.org/10.2305/IUCN.UK.20193.RLTS.T60169A124447127.en
Pollom R, Ebert DA, Fennessy S, Fernando S, Gledhill K, Kuguru B, Samoilys M (2019) *Rhinobatos holcorhynchus.* The IUCN Red List of Threatened Species 2019: T161405A124479447. https://dx.doi.org/10.2305/IUCN.UK.20193.RLTS.T161405A124479447.en
R Core Team (2021) R: a language and environment for statistical computing. R Foundation for Statistical Computing, Vienna. www.R-project.org/
Rutledge KM (2019) A new guitarfish of the genus *Pseudobatos* (Batoidea: Rhinobatidae) with key to the guitarfishes of the Gulf of California. Copeia 107:451–463
Séret B (2022) Marine and coastal ecosystems. Chondrichthyan fishes (sharks, rays and chimaeras). In: Goodman SM (ed) The new natural history of Madagascar. Princeton University Press, Princeton, NJ, p 386–398
Séret B, Carvalho MR (2022) Order Rhinopristiformes. Family Rhinobatidae. Guitarfishes and shovelnose rays. In: Heemstra PC, Heemstra E, Ebert DA, Holleman W, Randall JE (eds) Coastal fishes of the western Indian Ocean, Vol 1. National Research Foundation & South African Institute for Aquatic Biodiversity, Makhanda, p 564–571
Séret B, Last PR, Naylor GJP (2016) Guitarfishes. Family Rhinobatidae. In: Last PR, White WT, de Carvalho ME, Séret B, Stehmann MFW, Naylor GJP (eds) Rays of the world. Cornell University Press, Ithaca, NY, p 77–109
Simpfendorfer CA, Heupel MR, White WT, Dulvy NK (2011) The importance of research and public opinion to conservation managements of sharks and rays: a synthesis. Aust J Mar Freshwater Res 62:518–527
Smith JLB (1949) The sea fishes of Southern Africa. South Africa Central News Agency, Cape Town
Smith JLB (1961) The sea fishes of Southern Africa, 4th edn. Central News Agency, Cape Town
Smith JLB (1965) The sea fishes of Southern Africa, 5th edn. Central News Agency, Cape Town
von Bonde C, Swart DB (1923) The Platosomia (skates and rays) collected by the S. S. 'Pickle'. University of South Africa. Fish Mar Biolog Surv Rep 3:1–22
Wallace JH (1967) The batoid fishes of the East Coast of Southern Africa Part I: sawfishes and guitarfishes. In: Oceanographic Research Institute Investigational Report No. 15. Oceanographic Research Institute, Durban
Weigmann S (2011) Contribution to the taxonomy and distribution of eight ray species (Chondrichthyes, Batoidea) from coastal waters of Thailand. Verh Naturwiss Ver Hamburg 46:249–312
Weigmann S (2016) Annotated checklist of the living sharks, batoids and chimaeras (Chondrichthyes) of the world, with a focus on biogeographical diversity. J Fish Biol 88: 837–1037
Weigmann S, Ebert DA, Séret B (2021) Resolution of the *Acroteriobatus leucospilus* species complex, with a redescription of *A. leucospilus* (Norman, 1926) and descriptions of two new western Indian Ocean species of *Acroteriobatus* (Rhinopristiformes, Rhinobatidae). Mar Biodivers 51:58

Editorial responsibility: Paula B. Carlson (Guest Editor), Dallas, Texas, USA
Reviewed by: R. Misawa and 2 anonymous referees

Submitted: February 21, 2023
Accepted: October 11, 2023
Proofs received from author(s): December 19, 2023